Atmospheric
Chemistry
and Physics

Inverse modeling of GOSAT-retrieved ratios of total column CH$_4$ and CO$_2$ for 2009 and 2010

Sudhanshu Pandey[1,2], Sander Houweling[1,2], Maarten Krol[1,2,3], Ilse Aben[2], Frédéric Chevallier[4], Edward J. Dlugokencky[5], Luciana V. Gatti[6], Emanuel Gloor[7], John B. Miller[5,8], Rob Detmers[2], Toshinobu Machida[9], and Thomas Röckmann[1]

[1]Institute for Marine and Atmospheric Research Utrecht, Utrecht University, Utrecht, the Netherlands
[2]SRON Netherlands Institute for Space Research, Utrecht, the Netherlands
[3]Department of Meteorology and Air Quality (MAQ), Wageningen University and Research Centre, Wageningen, the Netherlands
[4]Laboratoire des Sciences du Climat et de l'Environnement (LSCE), CEA CNRS UVSQ, IPSL, Gif-sur-Yvette, France
[5]NOAA Earth System Research Laboratory, Boulder, Colorado, USA
[6]Instituto de Pesquisas Energéticas e Nucleares (IPEN), Centro de Química Ambiental, São Paulo, Brazil
[7]School of Geography, University of Leeds, Leeds, UK
[8]Cooperative Institute for Research in Environmental Sciences (CIRES), University of Colorado, Boulder, Colorado, USA
[9]National Institute for Environmental Studies, Tsukuba, Japan

Correspondence to: Sudhanshu Pandey (s.pandey@uu.nl)

Abstract. This study investigates the constraint provided by greenhouse gas measurements from space on surface fluxes. Imperfect knowledge of the light path through the atmosphere, arising from scattering by clouds and aerosols, can create biases in column measurements retrieved from space. To minimize the impact of such biases, ratios of total column retrieved CH$_4$ and CO$_2$ (X$_{ratio}$) have been used. We apply the ratio inversion method described in Pandey et al. (2015) to retrievals from the Greenhouse Gases Observing SATellite (GOSAT). The ratio inversion method uses the measured X$_{ratio}$ as a weak constraint on CO$_2$ fluxes. In contrast, the more common approach of inverting proxy CH$_4$ retrievals (Frankenberg et al., 2005) prescribes atmospheric CO$_2$ fields and optimizes only CH$_4$ fluxes.

The TM5–4DVAR (Tracer Transport Model version 5–variational data assimilation system) inverse modeling system is used to simultaneously optimize the fluxes of CH$_4$ and CO$_2$ for 2009 and 2010. The results are compared to proxy inversions using model-derived CO$_2$ mixing ratios (XCO$_2^{model}$) from CarbonTracker and the Monitoring Atmospheric Composition and Climate (MACC) Reanalysis CO$_2$ product. The performance of the inverse models is evaluated using measurements from three aircraft measurement projects.

X$_{ratio}$ and XCO$_2^{model}$ are compared with TCCON retrievals to quantify the relative importance of errors in these components of the proxy XCH$_4$ retrieval (XCH$_4^{proxy}$). We find that the retrieval errors in X$_{ratio}$ (mean = 0.61 %) are generally larger than the errors in XCO$_2^{model}$ (mean = 0.24 and 0.01 % for CarbonTracker and MACC, respectively). On the annual timescale, the CH$_4$ fluxes from the different satellite inversions are generally in agreement with each other, suggesting that errors in XCO$_2^{model}$ do not limit the overall accuracy of the CH$_4$ flux estimates. On the seasonal timescale, however, larger differences are found due to uncertainties in XCO$_2^{model}$, particularly over Australia and in the tropics. The ratio method stays closer to the a priori CH$_4$ flux in these regions, because it is capable of simultaneously adjusting the CO$_2$ fluxes. Over tropical South America, comparison to independent measurements shows that CO$_2$ fields derived from the ratio method are less realistic than those used in the proxy method. However, the CH$_4$ fluxes are more realistic, because the impact of unaccounted systematic uncertainties is more evenly distributed between CO$_2$ and CH$_4$. The ratio inver-

sion estimates an enhanced CO_2 release from tropical South America during the dry season of 2010, which is in accordance with the findings of Gatti et al. (2014) and Van der Laan et al. (2015).

The performance of the ratio method is encouraging, because despite the added nonlinearity due to the assimilation of X_{ratio} and the significant increase in the degree of freedom by optimizing CO_2 fluxes, still consistent results are obtained with respect to other CH_4 inversions.

1 Introduction

Detailed knowledge of the global distribution of surface fluxes of potent greenhouse gases (GHGs) such as CH_4 and CO_2 is needed to investigate the uncertain feedback of the global carbon cycle to human disturbances. Atmospheric measurements of these GHGs can provide information about the atmospheric budget. Inverse modeling methods, also known as top-down approaches, have been developed to make use of that information to obtain improved estimates of surface fluxes. Bottom-up estimates of those fluxes are used as prior values in the top-down method, and are further improved using atmospheric measurements. Inversions assimilating flask and/or in situ measurements from surface networks have significantly improved our knowledge of the sources and sinks of GHGs (Bousquet et al., 2006; Bergamaschi et al., 2010; Hein et al., 1997; Houweling et al., 1999; Peters et al., 2007; Chevallier et al., 2010; Gurney et al., 2008). However, many regions with a key role in the global annual budgets of CO_2 and CH_4 are not adequately covered by the surface measurement network. This is especially true for tropical regions and the Southern Hemisphere.

The Greenhouse Gases Observing SATellite (GOSAT) is the first satellite dedicated to monitoring GHGs from space (Kuze et al., 2009; Yokota et al., 2009; Yoshida et al., 2011). Onboard are the Thermal And Near infrared Sensor for carbon Observation-Fourier Transform Spectrometer (TANSO-FTS) and a dedicated Cloud and Aerosol Imager (TANSO-CAI). TANSO-FTS measures the absorption spectra of Earth-reflected sunlight in the shortwave infrared (SWIR) spectral range, from which XCO_2 and XCH_4 are retrieved with global coverage. Several inverse modeling studies have applied these measurements to derive constraints on the surface fluxes of CH_4 and CO_2 (Alexe et al., 2015; Basu et al., 2013; Deng et al., 2014; Maksyutov et al., 2012; Bergamaschi et al., 2013; Fraser et al., 2013; Houweling et al., 2015; Monteil et al., 2013; Turner et al., 2015).

Systematic errors in satellite retrievals are an important factor limiting the scientific interpretation of the data, and various methods have been proposed to mitigate their impact on the inferred surface fluxes (Bergamaschi et al., 2007; Frankenberg et al., 2005; Butz et al., 2010; Parker et al., 2015). An important source of systematic error is the scat-

tering of light by aerosols and thin cirrus clouds along the measured light path. Two types of retrieval methods have been developed in the past to account for atmospheric scattering, referred to as the full-physics and proxy approach. The full-physics approach tries to account for scattering-induced errors by explicitly modeling the scattering process, and retrieving scattering properties from the data (Butz et al., 2010). The proxy method, first introduced by Frankenberg et al. (2005), takes the ratio of XCH_4 and XCO_2 retrieved at nearby wavelengths (1562 to 1585 nm for XCO_2 and 1630 to 1670 nm for XCH_4) so that path length perturbations due to atmospheric scattering largely cancel out in the ratio (see Eq. 1). X_{ratio} is multiplied with model-derived XCO_2 (XCO_2^{model}) to derive XCH_4 (XCH_4^{proxy}) (see Eq. 2).

$$X_{ratio} = \frac{XCH_4^{ns}}{XCO_2^{ns}} \tag{1}$$

$$XCH_4^{proxy} = X_{ratio} \times XCO_2^{model} \tag{2}$$

Here, XCH_4^{ns} and XCO_2^{ns} are retrieved assuming a non-scattering atmosphere. XCO_2^{model} is calculated using a transport model, normally employing CO_2 surface fluxes that have been optimized using surface measurements. The atmospheric CO_2 fields are sampled at the coordinates of the satellite measurements and converted to corresponding total columns using the retrieval-derived averaging kernels (Schepers et al., 2012).

Proxy XCH_4 retrievals from GOSAT have been used in many inverse modeling studies to investigate the global surface fluxes of CH_4 (Alexe et al., 2015; Monteil et al., 2013; Fraser et al., 2013; Bergamaschi et al., 2013). These studies rely on the assumption that the uncertainties and biases in XCO_2^{model} are relatively unimportant. Some recent studies have investigated this assumption in further detail. Schepers et al. (2012) suggested that the errors in XCH_4^{proxy} are mostly dominated by the errors in XCO_2^{model}. Pandey et al. (2015) did a series of Observing System Simulation Experiments to quantify the impact of errors in XCO_2^{model} on inversion-derived CH_4 fluxes. It was concluded that the error becomes significant when CO_2 fluxes are poorly constrained by the surface measurements. Parker et al. (2015) have estimated the uncertainty in XCO_2^{model} by comparing values from different models. They found that the uncertainty in XCO_2^{model} becomes the most important term in the error budget of XCH_4^{proxy} retrieval during summer months, when the satellite instrument operates under favorable illumination conditions, allowing accurate determination of X_{ratio}.

In an attempt to avoid the biases introduced by errors in XCO_2^{model}, Fraser et al. (2014) developed the ratio method, which simultaneously constrains CO_2 and CH_4 fluxes by assimilating X_{ratio} on the subcontinental scale using the ensemble Kalman filter. Pandey et al. (2015) also developed a similar ratio inversion method for jointly optimizing the

surface fluxes of CH_4 and CO_2 on the model grid scale using a variational optimization method. Fraser et al. (2014) compared posterior CH_4 and CO_2 flux uncertainties derived from a ratio inversion with traditional CH_4 proxy and CO_2 full-physics inversions and reported a larger reduction in uncertainty than the two in the tropics for the fluxes of both tracers.

This study extends the work of Pandey et al. (2015), by separately inverting real GOSAT measurements of X_{ratio} and XCH_4^{proxy} in a consistent and comparable framework to investigate the following questions. (1) How do errors in XCO_2^{model} influence the results of a XCH_4^{proxy} inversion? (2) How does the X_{ratio} inversion system developed by Pandey et al. (2015) perform using real data? The performance of the inversions is evaluated using independent aircraft measurements. We provide an estimate of the posterior uncertainties of the X_{ratio}-inverted fluxes using the Monte Carlo method described by Chevallier et al. (2007).

This paper is organized as follows. The following section explains the methods used in this study. Section 2.1 describes the inverse model and the a priori flux assumptions. Section 2.2 lists the measurements that are assimilated in the inversions and used for validation. Section 2.3 provides an overview of the inversions performed in the study. Section 3 presents the inversion results and Sect. 4 discusses their implications for the use of satellite retrievals in inversion studies. Finally, we give the overall conclusions of this work.

2 Method

We invert GOSAT retrievals of X_{ratio} and XCH_4^{proxy}, each together with flask-air CH_4 and CO_2 measurements from the NOAA Global Greenhouse Gas Reference Network (GGGRN) to provide monthly surface fluxes of CO_2 and CH_4 using the TM5–4DVAR inversion system (Meirink et al., 2008). This is done as follows.

1. GOSAT-retrieved total column measurements of X_{ratio} are compared to measured ratios of $XCH_4 : XCO_2$ from the Total Carbon Column Observing Network (TCCON) of ground-based sun-tracking Fourier transform spectrometers (FTSs) (Wunch et al., 2011).

2. GOSAT X_{ratio} measurements are bias corrected by fitting a linear function of surface albedo to the residual differences between GOSAT and TCCON. This is done in X_{ratio} space.

3. GOSAT X_{ratio} measurements are multiplied by XCO_2^{model} to generate XCH_4^{proxy} measurements. Two different versions of XCO_2^{model} are used (see Sect. 2.2) to investigate the sensitivity to model errors.

4. The XCH_4^{proxy} and X_{ratio} measurements are inverted along with surface observations and the resulting posterior surface fluxes are integrated over the TransCom regions (see Fig. S4 in the Supplement).

5. The posterior flux uncertainty for all inversions is quantified using a Monte Carlo approach (see Appendix B) for consistent comparison.

6. The performance of the inversions is evaluated and compared using independent aircraft measurements.

The remainder of this section explains these steps in further detail.

2.1 Inversion setup

We use the TM5–4DVAR inversion modeling system. It is comprised of the Tracer Transport Model version 5 (TM5; Krol et al., 2005) coupled to a variational data assimilation system (4DVAR; Meirink et al., 2008). TM5 simulates the spatiotemporal distribution of a tracer in the atmosphere for a given set of fluxes. In this study, TM5 is run at a $6° \times 4°$ horizontal resolution and 25 vertical hybrid sigma pressure levels from the surface to the top of the atmosphere. The meteorological fields for this offline model are taken from the European Centre for Medium-Range Weather Forecasts (ECMWF) ERA-Interim reanalysis (Dee et al., 2011).

CH_4 fluxes are optimized as a single flux category, representing the sum of all processes. For CO_2, biospheric and oceanic fluxes are optimized separately. The a priori CH_4 fluxes used in the study are the same as used in Houweling et al. (2014), except for the anthropogenic fluxes. We use the v.4.2FT2010 version of EDGAR (European Commission, Joint Research Centre (JRC)/Netherlands Environmental Assessment Agency), whereas Houweling et al. (2014) use version 4.1. The a priori CO_2 fluxes come from CarbonTracker, CT2013B (Peters et al., 2007), in which biosphere fluxes are based on the Carnegie-Ames-Stanford Approach (CASA) biogeochemical model, fire fluxes are based on the Global Fire Emissions Database v3.1 (GFED), and ocean fluxes are based on Jacobson et al. (2007). Fossil fuel fluxes in CarbonTracker are based on the Miller module (Tans et al., 2014). The a priori flux covariance matrix is constructed assuming relative flux uncertainties of 50, 84, and 60 % per grid box and month for the total CH_4, biospheric CO_2, and oceanic CO_2 categories, respectively. The fluxes are assumed to be correlated temporally using an exponential correlation function with temporal scales of 3, 3, and 6 months, respectively, and spatially with Gaussian functions using corresponding length scales of 500, 500, and 3000 km for total CH_4, biospheric CO_2, and oceanic CO_2, respectively.

2.2 Measurements

Here we give a brief account of the measurements that were assimilated (GOSAT and NOAA) or used for validation (TCCON and aircraft measurements).
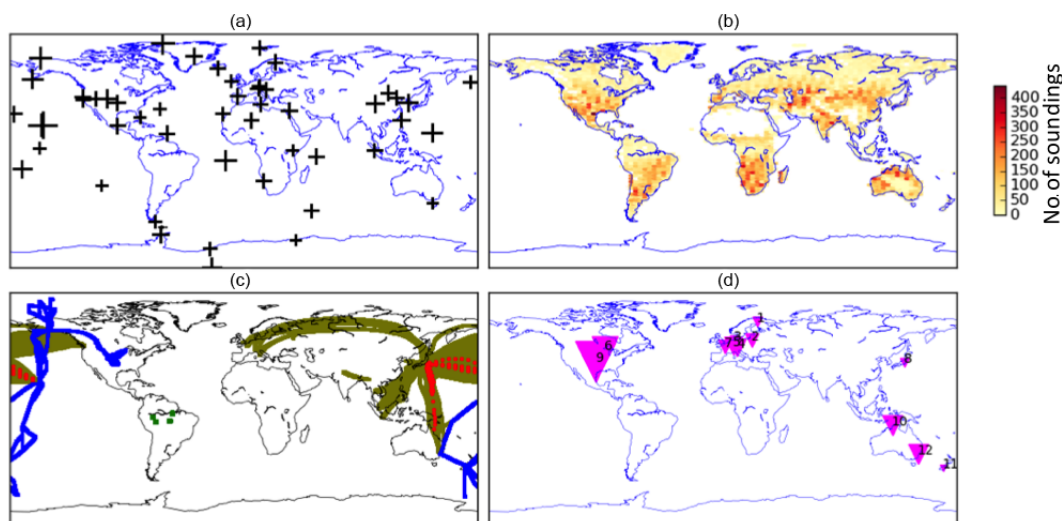
Figure 1. Measurements used in this study. **(a)** The crosses indicate the locations of NOAA surface sampling sites. The lengths of the vertical and horizontal bars are proportional to the number of CO_2 and CH_4 measurements, respectively. **(b)** The number of GOSAT soundings binned at $1° \times 1°$ for the time period of June 2009 to December 2010; **(c)** flight tracks of the aircraft campaigns HIPPO 2 and 3 (blue), CONTRAIL CO_2 (olive), CONTRAIL CH_4 (red), and AMAZONICA (green); **(d)** the locations of the TCCON measurement sites. The numbers (1–12) refer to corresponding entries in Table 1. The size of the purple rectangles is proportional to the number of collocated high-gain GOSAT soundings.

2.2.1 GOSAT

The XCH_4^{ns} and XCO_2^{ns} terms in Eq. (1) were taken from the RemoTeC XCH_4 Proxy retrieval v2.3.5 (Butz et al., 2011). More information about the data set can be found in the Product User Guide on the ESA GHG CCI website (Detmers and Hasekamp, 2014). The RemoTeC algorithm uses GOSAT TANSO-FTS NIR and SWIR spectra to retrieve XCH_4^{ns} and XCO_2^{ns} simultaneously, assuming a non-scattering atmosphere (Schepers et al., 2012). X_{ratio} values were translated into XCH_4^{proxy} using XCO_2^{model} derived from the following: (1) Monitoring Atmospheric Composition and Climate (MACC) reanalysis CO_2 product (www.copernicus-atmosphere.eu). It uses Laboratoire de Météorologie Dynamique transport model (LMDZ) (Chevallier, 2013). The corresponding XCH_4^{proxy} product will be referred to as XCH_4^{ma}. (2) XCO_2^{model} is derived from CarbonTracker-2013B (http://www.esrl.noaa.gov/gmd/ccgg/carbontracker/). These CO_2 fields are calculated using the TM5 model as used in this study. The corresponding XCH_4^{proxy} product will be referred to as XCH_4^{ct}.

Both data assimilation systems optimized the CO_2 fluxes using surface measurements of CO_2. For GOSAT measurements, we only used the high-gain soundings from GOSAT under cloud-free conditions from nadir mode. This was done to avoid any systematic inconsistency among the operation modes of TANSO. Figure 1 shows the spatial coverage of the GOSAT data set used in our inversions.

Systematic mismatches between NOAA-optimized and GOSAT-optimized TM5 CH_4 fields were observed by Mon-

teil et al. (2013). We apply another bias correction (in addition to TCCON-based bias correction applied to X_{ratio}) to X_{ratio} and XCH_4^{proxy} by comparing them to total column CH_4 and CO_2 optimized via an inversion using TM5–4DVAR and NOAA flask-air data (see Appendix A).

2.2.2 TCCON

TCCON is a global network of ground-based FTS instruments for measuring the total column abundance of several gases, including XCO_2 and XCH_4, in the near infrared region of the electromagnetic spectrum (Wunch et al., 2011). These measurements are the standard for validating total column retrievals from greenhouse-gas-observing satellites such as GOSAT. We validate XCH_4^{ns}, XCO_2^{ns}, X_{ratio}, XCO_2^{ma}, and XCO_2^{ct} with corresponding values of XCH_4, XCO_2, and $XCH_4 : XCO_2$ measured by TCCON at 12 sites using the GGG2014 release of the TCCON data set (see Fig. 1 and Sect. 3.1). An albedo-based bias correction was applied to GOSAT-retrieved X_{ratio} to account for the mismatch with TCCON X_{ratio} (see Appendix A).

2.2.3 NOAA

High-accuracy surface measurements of CH_4 and CO_2 were used from NOAA's GGGRN (Dlugokencky et al., 2015). The standard scale used for CO_2 is the WMO X2007 scale and for CH_4 is the WMO X2004 scale. Only the sites with continuous data coverage (on a roughly weekly basis) without gaps in the time period of 1 June 2009 to 31 December 2010 were included. A total of 8552 CH_4 observations and 7843 CO_2

Table 1. TCCON validation of the components of XCH_4^{proxy} (see Eq. 2). The numbers represent mean percentage differences with TCCON (weighted with TCCON + GOSAT error). A negative number means that the satellite retrieval is lower than TCCON. Data from these stations were used: Sodankylä (Kivi et al., 2014), Białystok (Deutscher et al., 2014a), Bremen (Deutscher et al., 2014b), Garmisch (Sussmann and Rettinger, 2014), Karlsruhe (Hase et al., 2014), Parkfalls (Wennberg et al., 2014a), Orleans (Warneke et al., 2014), Tsukuba (Morino et al., 2014), Lamont (Wennberg et al., 2014b), Darwin (Griffith et al., 2014a), Lauder (Sherlock et al., 2014), and Wollongong (Griffith et al., 2014b), and are arranged from north to south (for TCCON site locations, see Fig. 1).

Station	No. of collocated measurements	Mean differences with TCCON (%)				
		XCO_2^{ns}	XCH_4^{ns}	X_{ratio}	XCO_2^{ct}	XCO_2^{ma}
Sodankylä	434	−3.03	−2.81	0.21	0.68	0.34
Białystok	731	−2.46	−1.79	0.62	0.31	0.05
Bremen	426	−1.81	−0.99	0.76	−0.05	−0.32
Garmisch	1295	−1.93	−1.09	0.76	0.40	0.05
Karlsruhe	1244	−1.74	−1.00	0.69	0.15	−0.25
Parkfalls	2174	−1.23	−0.43	0.75	0.22	0.11
Orleans	808	−1.53	−0.75	0.75	0.21	−0.09
Tsukuba	135	−1.87	−1.24	0.63	0.57	−0.03
Lamont	5617	−0.73	−0.03	0.68	0.07	−0.00
Darwin	1065	−0.67	−0.19	0.47	0.02	0.14
Lauder	110	−1.05	−0.57	0.46	0.14	0.03
Wollongong	1515	−0.81	−0.45	0.35	0.10	0.00

observations were used from the same 51 sites. Figure 1 shows the location of the observation sites. 1σ uncertainties of 0.25 ppm and 1.4 ppb were assigned to CO_2 and CH_4 measurements, respectively (Basu et al., 2013; Houweling et al., 2014). Note that our system also assigns a modeling error to each observation depending on simulated local gradients in mixing ratio (Basu et al., 2013). Modeling error values have a mean of 27.5 ppb, 2.72 ppm (and 1σ of 25.5 ppb, 4 ppm) for CH_4 and CO_2, respectively.

2.2.4 Aircraft measurements

Airborne measurements from various aircraft measurement projects were used to test the inversion optimized model (see Sect. 3.2.5). The following projects have been used:

1. HIAPER Pole-to-Pole Observations (HIPPO) from Wofsy et al. (2012a);

2. Comprehensive Observation Network for TRace gases by AIrLiner (CONTRAIL) from Machida et al. (2008);

3. IPEN aircraft measurements over Brazil (referred as AMAZONICA) from Gatti et al. (2014).

HIPPO provides in situ measurements covering the vertical profiles of CO_2 and CH_4 over the Pacific, spanning a wide range in latitude (approximately pole-to-pole), from the surface up to the tropopause. We used data from the HIPPO 2 (26 October to 19 December 2009) and HIPPO 3 (20 March to 20 April 2010) campaigns. The continuous in situ measurements of CH_4 and CO_2 that were used have been bias corrected with flask-air samples that were collected during each flight and analyzed at NOAA (Wofsy et al., 2012b).This

allows us to make consistent comparison with our inversions models, as all of them assimilate NOAA flask measurements. CONTRAIL makes use of commercial airlines to measure in situ CO_2 by continuous measurement equipment. For some of the CONTRAIL flights CH_4 measurements are also available from flask-air samples. We use data from a lower-troposphere greenhouse-gas sampling program as part of the AMAZONICA project, over the Amazon Basin in 2010, measuring biweekly vertical profiles of CO_2 and CH_4 from above the forest canopy to 4.4 km above sea level at four locations: Tabatinga (TAB), RioBranco (RBA), Alta Floresta (ALF), and Santarem (SAN) (Gatti et al., 2014). The coverage of all aircraft measurements that were used in this study is shown in Fig. 1.

2.3 Inversion experiments

The following inversions have been performed:

1. SURF: inversions assimilating flask-air measurements of CH_4 or CO_2 to constrain surface fluxes of CH_4 or CO_2, respectively;

2. RATIO: inversion assimilating X_{ratio} and flask-air measurements of CH_4 and CO_2 to constrain surface fluxes of CH_4 and CO_2;

3. PR-MA: inversion assimilating proxy XCH_4^{ma} and flask-air measurements of CH_4 to constrain surface fluxes of CH_4;

4. PR-CT: inversion assimilating proxy XCH_4^{ct} and flask-air measurements of CH_4 to constrain surface fluxes of CH_4.

To assess the relative performance of each inversion, we validate atmospheric concentrations as simulated using the optimized fluxes from the different inversions with aircraft measurements. We define a normalized chi-square statistic to quantify the agreement between the optimized model and aircraft measurements.

$$\kappa = \frac{1}{n}(\boldsymbol{y} - \mathrm{Hx})^T \mathbf{R}^{-1} (\boldsymbol{y} - \mathrm{Hx}), \tag{3}$$

where $\boldsymbol{y}$ is a vector of the aircraft measurements, n is the length of $\boldsymbol{y}$. Hx is the TM5 simulation sampled at the measurement coordinates. The covariance matrix $\mathbf{R}$ represents the expected uncertainty in the model–data mismatch. Its diagonal elements are calculated as the sum of the model representation error of TM5 and the measurement uncertainty; all non-diagonal elements are set to 0.

3 Results

3.1 GOSAT–TCCON comparison

TCCON measurements are used to investigate the errors in GOSAT-retrieved XCH_4. Each term on the right-hand side of Eq. (2) contributes to the uncertainty in XCH_4^{proxy}. To quantify these error contributions, we compare TCCON measurements of X_{ratio}, XCH_4, and XCO_2 to corresponding co-located GOSAT-retrievals. The validation is carried out for the time period of 1 June 2009 to 31 December 2013, for which both proxy data sets (XCH_4^{ma} and XCH_4^{ct}) are available. Table 1 shows mean differences per TCCON station, expressed as fractional differences to facilitate the comparison of quantities with different units. As expected, the largest differences between GOSAT and TCCON are found for XCO_2^{ns} and XCH_4^{ns}. In general, XCO_2^{ns} (mean $= -1.57\%$) shows larger relative differences than XCH_4^{ns} (mean $= -0.95\%$). A latitudinal dependence can be observed, with increasing biases towards stations at higher latitudes. This can be explained by increased aerosol scattering at larger sun angles, as the light path through the atmosphere is longer. For all the stations, the mean difference is negative which is expected for aerosol scattering-induced errors at the low surface albedos of the TCCON sites (Houweling et al., 2004). The smaller bias values for X_{ratio} than XCO_2^{ns} and XCH_4^{ns} confirm that scattering-induced errors cancel out in their ratio, which motivated the proxy approach (Frankenberg et al., 2005). Overall, we observe that X_{ratio} (mean bias $= 0.59\%$) is the larger contributor to the error in XCH_4^{proxy} than MACC (XCO_2^{ma}, mean bias $= 0.01\%$) and CarbonTracker (XCO_2^{ct}, mean bias $= 0.24\%$).
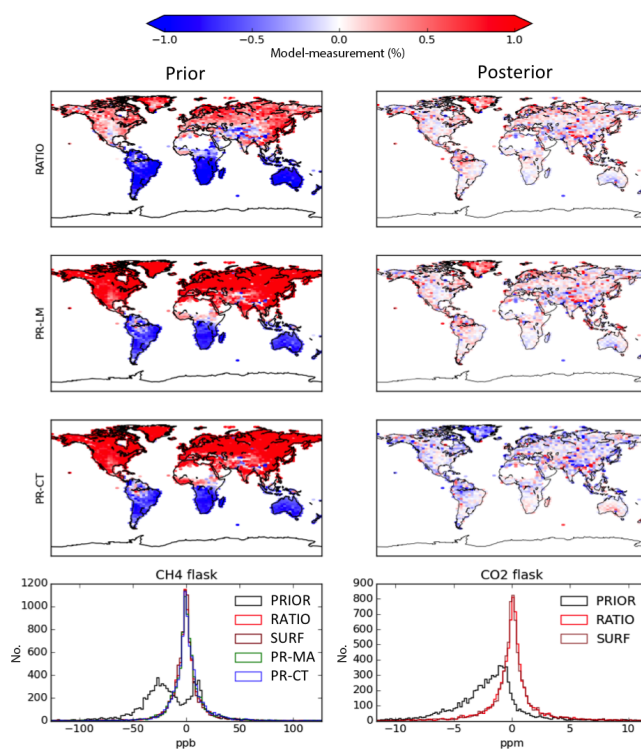

Figure 2. Fit residuals, comparing the performance of different inversions. The top three rows show the difference between TM5–4DVAR and GOSAT measurements (X_{ratio} for RATIO, XCH_4^{proxy} for PR-CT and PR-MA), using a priori (left) and a posteriori (right) fluxes. The bottom row shows histograms of measurement–model mismatches between TM5–4DVAR and NOAA surface measurements in 400 bins between $\pm 10\sigma$ range of the a priori mismatch.

3.2 Inversion results

3.2.1 Assimilation statistics

Figure 2 summarizes the statistics of the model–measurement comparison. The prior X_{ratio} mismatches typically fall in the range $\pm 1\%$ (with mean $= 0.007$ ppb/ppm and $1\sigma = 0.043$ ppb/ppm). The inversions reduce the average mismatch by about a factor of 10, and the variation of single column mismatches by about a factor of 2. The XCH_4^{proxy} of PR-CT and PR-MA have bimodal prior mismatches, because the a priori model overestimates the north–south gradient of CH_4. The bottom panels of Fig. 2 show mismatches between TM5 and surface flask measurements of CH_4 and CO_2. The CH_4 a priori measurement mismatch has a mean of -18.30 ppb and a 1σ of 42.30 ppb. The RATIO, SURF, PR-CT, and PR-MA inversions are all able to fit the NOAA data to a similar extent, reducing the a priori differences by more than a factor of 20. CO_2 flask measurements are assimilated in SURF and RATIO. Both inversions reduce the a priori mismatch (mean $= -2.12$ ppm, $1\sigma = 3.88$ ppm), with RATIO (mean $= -0.04$ ppm, $1\sigma = 3.69$ ppm) fitting
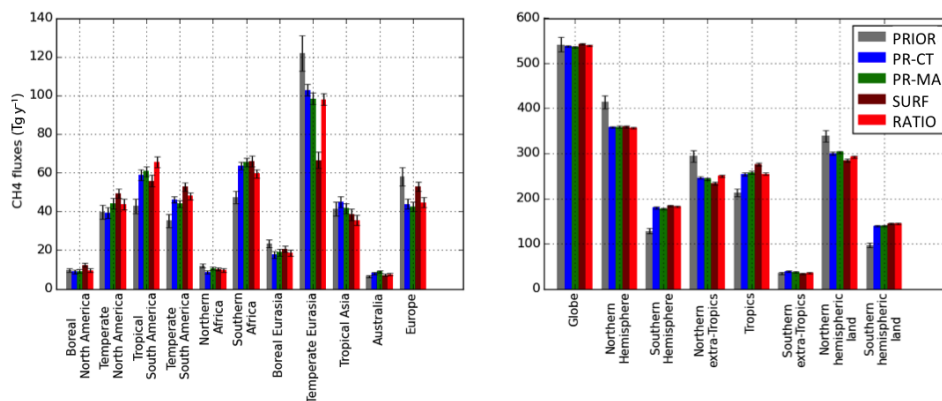
Figure 3. Annual fluxes of CH_4 integrated over different regions. The black line on each bar represents the $\pm 1\sigma$ uncertainty.

the CO_2 flask data as well as SURF (mean $= -0.06$ ppm, $1\sigma = 3.72$ ppm).

3.2.2 CH_4 fluxes

Optimized annual CH_4 fluxes, integrated over the TransCom regions are shown in the left panel of Fig. 3. The fluxes obtained with the RATIO inversion are on average more similar to fluxes from other GOSAT inversions than to the surface inversion, with a few exceptions. Differences between satellite and surface inversion are most prominent over tropical South America, where the latter is closer to the prior, which can likely be explained by the lack of surface measurement coverage. We will return to the inversion results for tropical South America in Sect. 3.2.6, where validation results are shown using aircraft data.

The most significant difference between the satellite inversion and SURF is found for temperate Eurasia, where SURF reduces the CH_4 fluxes from $121\,\mathrm{Tg\,y}^{-1}$ in the prior estimate to $66\,\mathrm{Tg\,y}^{-1}$. When satellite data are added, the fluxes increase again to $100\,\mathrm{Tg\,y}^{-1}$. The large flux correction in the SURF inversion is compensated by increases in other TransCom regions of $5–10\,\mathrm{Tg\,y}^{-1}$ (see for example temperate North and South America). In those regions satellite inversions remain closer to the prior than the SURF inversion, which may well be driven by the much smaller flux corrections for temperate Eurasia. The exception is Europe, where the satellite inversions show larger reductions of up to $15\,\mathrm{Tg\,y}^{-1}$. The large adjustments over temperate Eurasia are analyzed further in Sect. 3.2.7. PR-CT and PR-MA result in relatively similar posterior annual fluxes for all regions. RATIO is in good agreement with the proxy inversions except for tropical South America and southern Africa. The right panel of Fig. 3 shows annual fluxes integrated over large regions on the globe. We find a consistent adjustment in the north–south gradient of CH_4 compared to the prior in all inversions, corresponding to a flux shift from the Northern to the Southern Hemisphere of approximately $50\,\mathrm{Tg\,y}^{-1}$. This might be due to an overestimation of the a priori fluxes from

northern wetlands, as discussed in Spahni et al. (2011). A bias in inter-hemispheric transport in TM5 is not a likely cause, since the use of ECMWF-archived convective fluxes in TM5 has been shown to lead to a realistic simulation of the north–south gradient of SF6 (Van der Laan et al., 2015). Houweling et al. (2014) found similar CH_4 flux shifts between the hemispheres, after bringing the inter-hemispheric transport in agreement with SF6 using a parameterization of horizontal diffusion.

Next we shift focus to seasonal differences between the inversion-derived methane fluxes (see Fig. 4). Also on the seasonal scale, RATIO resembles the two PROXY inversions more than SURF. In boreal North America, the satellite inversions that assimilate GOSAT soundings are in better agreement with the prior. We observe an increase in summertime CH_4 fluxes in SURF estimates for boreal and temperate North America. The differences in annual mean fluxes discussed earlier for tropical South America and temperate Eurasia do not show a seasonal dependence. Large differences in seasonality are obtained for Australia and the African regions, which also show important differences between the two proxy inversions (see Sect. 3.2.4). In southern Africa, all inversions show increased CH_4 fluxes compared to the prior estimate; however, small differences can be seen between the two proxy inversions, especially in 2010. SURF remains in good agreement with PRIOR (a priori fluxes), which is expected as no surface observations are available to constrain the fluxes in this region.

3.2.3 CO_2 fluxes

Annual CO_2 fluxes from the SURF and RATIO inversions, integrated over TransCom regions, are shown in Fig. 5. Overall, we find good consistency between the results from RATIO and SURF except for temperate Eurasia, where RATIO results in a higher CO_2 uptake of $0.5\,\mathrm{PgC\,y}^{-1}$. Corresponding reductions in CH_4 fluxes are found for this region in the RATIO inversion. This can be understood by realizing that the satellite information that is used consists of the ratio of
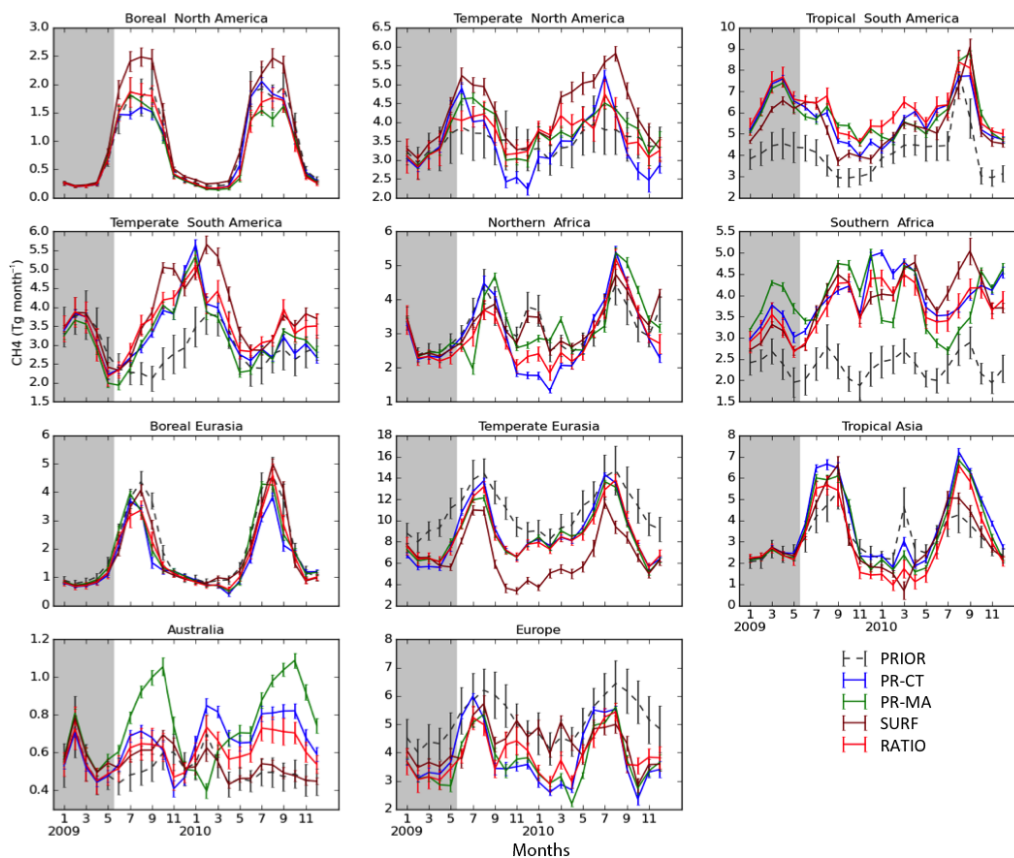
Figure 4. Monthly fluxes of CH_4 integrated over TransCom regions. The vertical lines represent a 1σ uncertainty of the monthly fluxes. The gray region in each plot represents the period in which no measurements are assimilated.
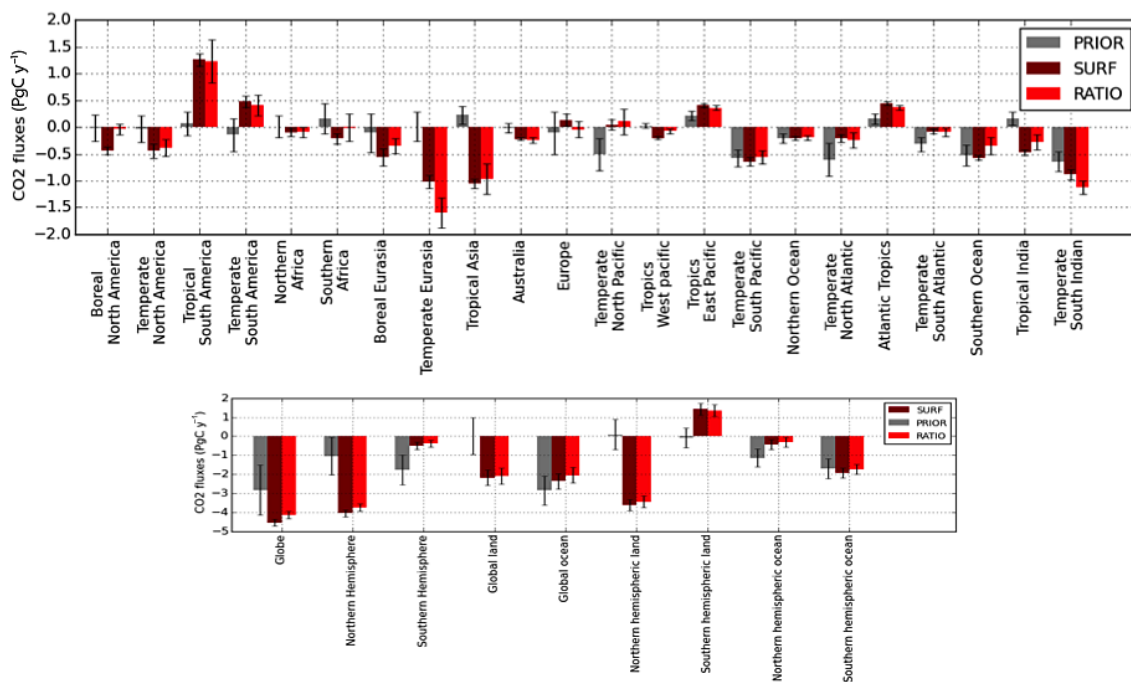

Figure 5. Annual fluxes of CO_2 (excluding fossil fuel emissions) integrated over different regions.

CH_4 and CO_2 columns. A RATIO inversion can simultaneously reduce the CO_2 and CH_4 fluxes over a region without changing the X_{ratio} in the atmosphere. SURF points towards a natural sink of $0.5\,PgC\,y^{-1}$ in boreal North America. RATIO and the a priori fluxes are carbon-neutral in this region. This agreement is also seen on the CH_4 side of the RATIO inversion. Only small differences between the posterior and prior fluxes of SURF and RATIO are found over the oceans except for the temperate North Pacific, which is neutral in both inversions compared to a sink of $-0.5\,PgC\,y^{-1}$ in the prior fluxes, and in tropical India which is turned into a net sink. Interestingly, RATIO leads to posterior fluxes for Europe that are close to carbon-neutral for the analysis period. This is in contrast with the findings of several inversions using GOSAT full physics XCO_2 retrievals, suggesting a largely underestimated European carbon sink of the order of $1\,PgC\,y^{-1}$ (Basu et al., 2014; Chevallier et al., 2014; Reuter et al., 2014; Houweling et al., 2015).

The RATIO and SURF inversions increase the global CO_2 sink of the terrestrial biosphere compared with the a priori fluxes. This is primarily caused by the bottom-up CASA model, which has been reported to underestimate the carbon uptake of the northern biosphere sink in the summer season (Yang et al., 2007). Basu et al. (2013) also find a global natural sink of 3 to $4\,PgC\,y^{-1}$ for GOSAT and NOAA inversions. This natural sink is needed to fit the atmospheric growth rate of CO_2 in the presence of about $9\,PgC\,y^{-1}$ anthropogenic emissions. The Southern Hemisphere land is turned into a source of $1\,PgC\,y^{-1}$ in both inversions.

3.2.4 Errors in CO_2^{model}

In this section, we analyze the differences between the two proxy retrievals (XCH_4^{ct} and XCH_4^{ma}) and how they propagate into posterior CH_4 fluxes. Note that these differences arise only from differences in XCO_2^{model}, and therefore large differences between the XCH_4^{proxy} measurements point towards high uncertainties in the model representations of atmospheric CO_2. Figure 6 further displays the result of these inversions. We find a mean difference between XCH_4^{ma} and XCH_4^{ct} of $-2.36\,ppb$ and a 1σ of $4.55\,ppb$. This is caused by mean differences between XCO_2^{ma} and XCO_2^{ct} of $-0.50\,ppm$ and a σ of $0.97\,ppm$ (not shown in the figure). We find a seasonal variation in the difference with the largest amplitudes of about $10\,ppb$ in the northern tropics. The phasing varies with latitude, with positive values during boreal summer to autumn. The smallest differences are found in the Southern Hemisphere. Figure 6b shows how this seasonal pattern propagates into the posterior CH_4 fluxes. The seasonal and latitudinal variation in the CH_4 flux difference follows the variation in the XCH_4^{proxy} difference, with an amplitude of $0.5\,Tg\,month^{-1}\,gridcell^{-1}$. The regions without satellite data coverage, i.e., below $60°\,S$ and above $60°\,N$, show smaller differences in the optimized fluxes.
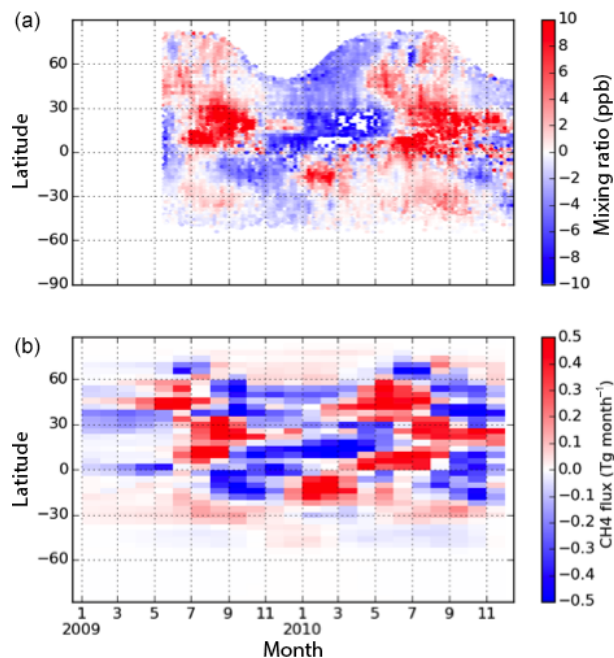

Figure 6. (a) Zonally averaged differences in CH_4 column mixing ratio between the two XCH_4^{proxy} retrievals (XCH_4^{ma}–XCH_4^{ct}). **(b)** Corresponding differences in a posteriori CH_4 flux between the proxy inversions using these data (PR-MA minus PR-CT).

PR-CT and PR-MA yield different CH_4 fluxes in northern Africa and Australia (see Fig. 4). We plot these fluxes with the corresponding regional averaged XCH_4 values in Fig. 7. For northern Africa, the difference in XCH_4^{proxy} of up to $10\,ppb$ around January 2010 gives rise to a difference in the monthly posterior flux of $1\,Tg\,month^{-1}$. In Australia, XCH_4^{ma} and XCH_4^{ct} are in relatively good agreement with each other, with differences within $2\,ppb$. However, because the a priori fluxes from this region are very small, the difference in the optimized seasonal cycle of fluxes nevertheless becomes relatively large. In particular, PR-MA causes significant deviations from the a priori fluxes, with decreases in the posterior fluxes during Australian summer, and large increases during winter. Another reason for these flux adjustments is the limited land area in the Southern Hemisphere that is available for CH_4 flux adjustments (over the open ocean the a priori flux uncertainties are small, limiting their adjustment).

Detmers et al. (2015) reported an enhanced CO_2 sink over central Australia in the second half of 2010 lasting until 2012, caused by an increase in vegetation due to enhanced precipitation during La Niña conditions. If not properly represented in inversions using surface measurements, this negative CO_2 anomaly causes XCO_2^{model} to be overestimated. In that case, the anomaly propagates to the proxy retrievals, resulting in overestimation of XCH_4^{proxy}, leading to overestimated a posteriori CH_4 fluxes. RATIO estimates a significantly stronger sink of CO_2 in agreement with Detmers et al.
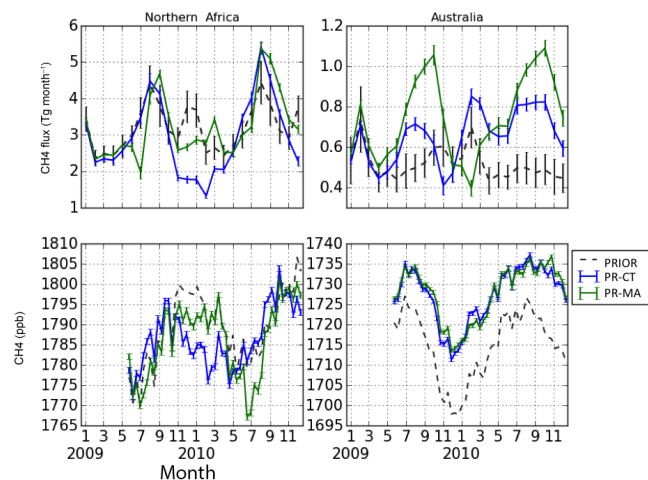
Figure 7. The top panels show the posterior monthly fluxes integrated over TransCom region. Bottom panels show the time series of the mean of XCH_4^{proxy} over northern Africa and Australia. The dotted line in the bottom panels denotes the mean of a priori modeled XCH_4 sampled at GOSAT sites.

(2015) (see Fig. S2 in the Supplement). This results in lower CH_4 fluxes in the RATIO inversion (see Fig. 4), demonstrating how the RATIO inversion method can avoid shortcomings in the proxy inversions in regions where CO_2 is poorly constrained by surface data.

PR-CT and PR-MA have opposite seasonal cycles, which may be due to their XCO_2^{model} components that are derived using different ecosystem models. CarbonTracker uses a priori natural fluxes from a CASA simulation driven by actual climatological information, whereas MACC uses only the climatology of natural fluxes. Therefore, the interannual variability of the inverted fluxes in MACC is driven by measurements only. Since the surface network does not pose strong constraints on the Australian carbon budget, the differences are driven by the prior fluxes of the two models, which may be more realistic in CarbonTracker in this case.

3.2.5 Aircraft validation

To further investigate the performance of our inversions, we validate the inversion-optimized CH_4 and CO_2 mixing ratios against independent aircraft measurements obtained during the projects described in Sect. 2.2. The results of the HIPPO and CONTRAIL validation are shown in Fig. 8 and the values for κ for CH_4 and the root-mean-square difference (RMSD) for CO_2 are given in Fig. 9. κ values are not calculated for CO_2 because we do not have the CO_2 model representation errors used in MACC and CarbonTracker. More details on statistics of the validation are provided in Table S1 in the Supplement.

The difference between HIPPO and PRIOR reflects the overestimated north–south gradient that is found using a priori CH_4 fluxes, as already discussed in Sect. 3.2.2. In addi-

tion, PRIOR shows a uniform bias of 13.5 ppb. SURF and RATIO correct the north–south gradient and reduce biases to 5.56 and 6.68 ppb, respectively. All the models are performing equally well in terms of κ. The original MACC and CarbonTracker CO_2 fields have RMSD values of 1.08 and 1.09 ppm, respectively, which is lower than the RMSD of RATIO (1.64 ppm) and SURF (1.65 ppm). We suggest that CarbonTracker and MACC have a better representation of CO_2 than PR-CT, PR-MA, and SURF as they assimilate a larger number of flask measurements sites and also few continuous in situ sites.

Compared with the large CONTRAIL data set of CO_2 measurements, only a limited number of CH_4 measurements are available, mostly over the Pacific Ocean (see Fig. 1). We observe the same north–south gradient mismatch with PRIOR as seen in the comparison to HIPPO. PR-CT is able to improve the PRIOR κ of 6.99 to 4.56, followed in order of decreasing performance by PR-MA (4.71), SURF (5.33), and RATIO (5.47). The values of κ are larger than 1, which points to significant errors in all the inversion results. The RMSD of the different inversions are comparable. The large data set of CONTRAIL CO_2 measurements covers a much larger area, including flight tracks to Europe and southeast Asia. Our validation shows a mean error of 2.23 ppm in PRIOR. The NOAA and RATIO inversions reduce this bias to -0.43 and -0.41 ppm, respectively. However, similar to the HIPPO validation, MACC (mean bias $= -0.2$ ppm) and CarbonTracker-derived CO_2 (mean bias $= 0.11$ ppm) fields are in better agreement with the CONTRAIL measurements than the inversions.

3.2.6 Tropical South America

Tropical South America contains the Amazon Basin, which is a large reservoir of standing biomass and contains one of the largest wetlands in the world. Therefore, it plays an important role in the annual global budget of both CO_2 and CH_4. Inversion results for the region have been validated using AMAZONICA measurements (see Fig. S5 and Table S1 in the Supplement). Generally, the model results using PRIOR fluxes underestimate the measured CH_4 mixing ratios (mean offset $= -32.02$ ppb). All inversions correct this offset, with SURF performing best (mean mismatch $= -14.18$ ppb). RATIO closely follows SURF with a mean mismatch of -17.18 ppb. The proxy inversions have a higher mismatch than RATIO and SURF, with means of -20.30 and -24.11 ppb, respectively for PR-MA and PR-CT. The κ values for the AMAZONICA CH_4 measurements (see Fig. 9) again show that fluxes from RATIO lead to lower mismatches than those from PR-CT and PR-MA. RATIO predicts this region as a significantly high CH_4 source for the first half of 2010 (see Fig. 4), and is in good agreement with aircraft measurements.

To check whether this is caused by errors in XCO_2^{model}, we perform similar comparisons using AMAZONICA CO_2
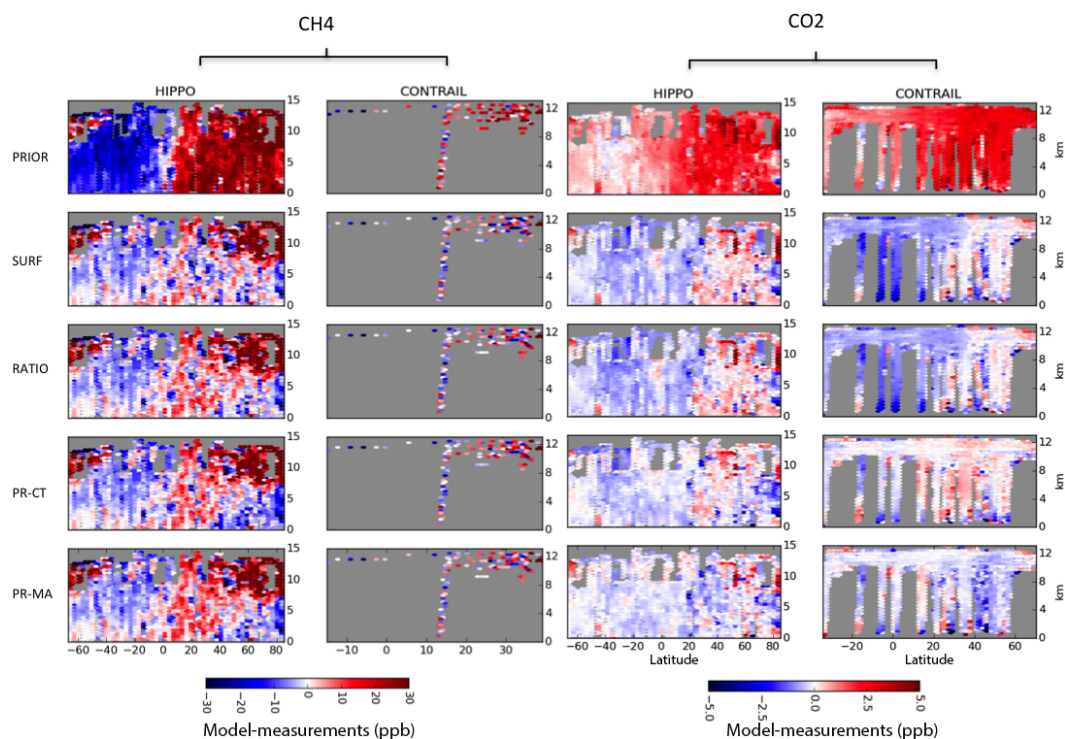
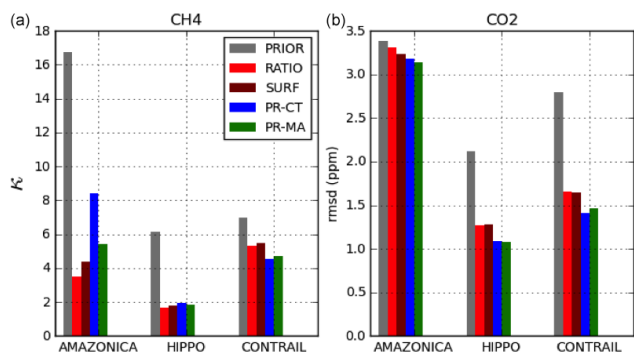**Figure 8.** Validation of inversion-optimized concentration fields of CO_2 and CH_4 with airborne measurements.

Figure 9. Summary of aircraft validation results per project for CH_4 (**a**, expressed as κ) and CO_2 (**b**, expressed as RMSD) for the whole inversion time period i.e., from 1 January 2009 to 31 December 2010.

measurements. We find that the two original models represent CO_2 about equally well in terms of RMSD (see Table S1 in the Supplement). Therefore, the higher mismatch of PR-CT and PR-MA for CH_4 is not due to a poor representation of the XCO_2^{model} over the region. This raises the question as to why RATIO performs better. In Sect. 3.1, we observe that the error in CO_2^{model} is generally lower than the error in the GOSAT X_{ratio} retrievals. In proxy inversions, this retrieval error, which is coming from X_{ratio} (see Eq. 2), is directly transferred to CH_4 fluxes, whereas in RATIO it is distributed over the CH_4 and CO_2 part of the state vector. The high posterior

CO_2 flux uncertainties for RATIO in the region support this further (see Fig. 5).

Flux maps of the region show that the satellite inversions provide a more spatially resolved adjustment of the CH_4 fluxes than SURF (see Fig. S3 in the Supplement). The satellite inversions estimate higher fluxes in the northwest corner of the region near Colombia. Similar increases have been reported in earlier studies, assimilating satellite-retrieved XCH_4 (Monteil et al., 2013; Frankenberg et al., 2006). The spatial pattern of the flux adjustment suggests that the proxy inversions compensate the increase over Colombia by reducing the fluxes in the Amazon Basin, which is less well covered by satellite retrievals due to frequent cloud cover. This may explain why the proxy inversions end up underestimating the observations inside the basin. SURF is mainly constrained by the large-scale inter-hemispheric gradient. This leads to a different pattern of flux adjustments, increasing only the fluxes in the southern part of the region while keeping the fluxes in Amazon Basin close to the prior. This solution brings SURF in relatively close agreement with the measurements. RATIO also shows a flux enhancement in Colombia, but at the same time represents the Amazon Basin better than the proxy inversions, likely because of its larger number of degrees of freedom in modifying regional flux patterns of both CO_2 and CH_4.

Gatti et al. (2014) and Van der Laan et al. (2015) reported an anomalous natural source of CO_2 in the region in 2010, also using AMAZONICA aircraft measurements. In this

study, RATIO predicts a more enhanced CO_2 natural source than the SURF and PRIOR. RATIO (RMSD = 3.23 ppm) is also in better agreement in terms of RMSD with AMAZON-ICA CO_2 data than SURF (RMSD = 3.31 ppm) and PRIOR (3.38 ppm). This demonstrates, like in the case of Australia, that the RATIO method is capable of informing us about the CO_2 fluxes, from which the CH_4 flux estimation benefits also.

3.2.7　Temperate Eurasia

As mentioned in Sect. 3.2.2, SURF leads to a drastic flux reduction in temperate Eurasia, whereas all satellite inversions show comparatively smaller decreases. Here, we investigate this in further detail by analyzing the inversion-optimized fits to the NOAA measurements at five surface sites located in this region (see Fig. 10). We find large mismatches between the a priori simulated concentrations and the measurement at these sites, with mean offsets ranging between 29.1 ppb at Mt. Waliguan and 174 ppb at Shangdianzi. All inversions correct for this mismatch by decreasing the regional fluxes. Surprisingly enough, the satellite inversions are able to fit the flask measurements even better than SURF, despite smaller corrections to the fluxes. For example, the mean posterior mismatch at Shangdianzi is 24.3 ppb for SURF, and only 7.5 to 9.8 ppb for the satellite inversions. A possible explanation is the double counting of surface data in the satellite inversions, as the satellite data have been bias corrected using an inversion that was already optimized using surface data. However, the bias correction is only applied as a zonal and annual mean. All inversions show similar reductions in the fluxes from eastern temperate Eurasia (mostly China) to match the NOAA measurements. However, the satellite inversions tend to compensate for this flux decrease over China by increased fluxes in India and the central part of temperate Eurasia.

4　Discussion

We have demonstrated that the application of the ratio method to GOSAT data yields realistic solutions for CO_2 and CH_4 fluxes. Its performance is comparable, and may in some regions even be better than the proxy inversion method. This is an important finding because the X_{ratio} retrieval approach provides a useful alternative to the full-physics method in that cloud filtering is less critical. In the case of GOSAT, it increases the number of useful measurements by about a factor of 2 (Butz et al., 2010; Fraser et al., 2014). At the same time, the RATIO inversion method avoids using the model-derived CO_2 fields as a hard constraint, which is an important limitation of the proxy method.

The realistic performance of the ratio method is certainly not a trivial outcome, since it prompts the user for specification of new uncertainties, influencing the way in which mea-
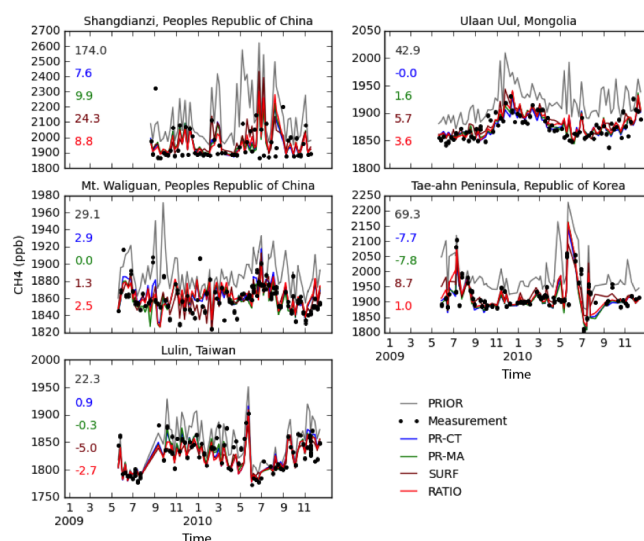

Figure 10. Inversion-optimized fits to surface measurement sites in temperate Eurasia. The numbers in the plots are the mean biases of models with measurements.

surement information is shared between CH_4 and CO_2. The joint CO_2 and CH_4 inversion problem has a larger number of degrees of freedom, as a result of which CH_4 flux adjustments can compensate for errors in CO_2 and vice versa. Assimilating surface measurements helps to decouple CH_4 and CO_2, which works best in regions that are relatively well covered by the surface network.

In other regions, the method can be improved further by accounting for correlations between a priori fluxes of CH_4 and CO_2. This study does not specify such correlations, which correspond to the assumption that a priori CO_2 and CH_4 flux uncertainties are independent of each other. Fraser et al. (2014) accounted for a priori uncertainty correlations for biomass burning fluxes of CO_2 and CH_4, based on the available information about emission ratios. Imposing such a priori constraints increased posterior uncertainty reduction compared to other methods for both CH_4 and CO_2 in some regions.

It is noteworthy that the inversions are run assuming uncorrelated measurements and a perfect transport. Also, as we are not optimizing the atmospheric sink of CH_4, all the information from its budget is used to constrain the surface fluxes. Hence, the estimates of posterior uncertainties tend to be optimistic in this study. The χ^2 statistic indicates whether the assumed measurement and prior errors are statistically consistent (Meirink et al., 2008). We find $\chi^2/n_s = 0.93$ for RATIO, 0.96 for PR-CT, 0.93 for PR-LM, and 1.14 for SURF in the CH_4 inversions (n_s is the number of observations assimilated in the inversion). This shows that we are not drastically underestimating the prior uncertainties in our CH_4 inversions.

One problem with the ratio method is the assimilation of X$_{ratio}$ over oceans. The uncertainty of CH$_4$ fluxes over the open oceans is relatively small. As a result, the model–data mismatch over the ocean is mostly accounted for by adjusting the CO$_2$ fluxes, which has a larger a priori uncertainty. At the same time, CO$_2$ fluxes over oceans tend to be very sensitive to small and systematic model–data mismatches of a few tenths of a ppm (Basu et al., 2013). Any bias in atmospheric transport, affecting both CO$_2$ and CH$_4$, is projected on the CO$_2$ fluxes, which may lead to rather unrealistic estimates of the annual CO$_2$ exchange over oceanic regions. Palmer et al. (2006) proposed to account for cross correlations in the model representation error between the components of a dual tracer inversion, which could reduce the extent of this problem.

Our surface-only inversion shows a large decrease in the fluxes from temperature Eurasia. To better understand this, we look at results of other recently published CH$_4$ inversion results. We group the studies into three groups: (1) studies not using EDGAR v4.2 as a priori fluxes, comprising Houweling et al. (2014), Monteil et al. (2013), Bruhwiler et al. (2014), and Fraser et al. (2013); (2) studies using EDGAR v4.2 but not assimilating the Shangdianzi site, comprising Alexe et al. (2015) and Bergamaschi et al. (2013); (3) studies using EDGAR v4.2 and assimilating Shangdianzi site comprising this work and Thompson et al. (2015). The inversions of group 1 do not show a systematic reduction in fluxes of temperate Eurasia. Inversions of group 3 tend to reduce the fluxes from the region the most; whereas, group 2 reduces fluxes by an intermediate amount. This outcome is partly explained by the EDGAR 4.2 fluxes being substantially higher in temperate Eurasia than previous EDGAR versions, as found also by Bergamaschi et al. (2013). In addition, however, these increased fluxes have the largest impact on surface-only inversions assimilating measurements from the Shangdianzi site, possibly due to a nearby hotspot in EDGAR v4.2. The hotspot is located near Jiexiu in the Shanxi province (112° E, 37° N), and has coal emissions of 10.83 Tg y^{-1} for the year 2010 from a 10×10 km grid. According to the EDGAR team (G. Meanhout, personal communication, 2015), this unrealistically high local source of CH$_4$ is the consequence of disaggregating large emission from Chinese coal mining using the limited available information on the location of the coal mines. Thompson et al. (2015), the other study in group 3, show a large a priori mismatch with a root-mean-square error of 103 ppb at Shangdianzi. Their inversions reduce their a priori east Asian CH$_4$ fluxes of 82 Tg y^{-1} by 23 Tg y^{-1}, with large adjustments in the fluxes from rice cultivation. Further research is needed to investigate the implications of the shortcomings of EDGAR v4.2. It is noteworthy, however, that when satellite data are assimilated in these studies, the improved regional coverage reduces the impact of this local disaggregation problem on the estimated regional fluxes.

5 Conclusions

This study investigated the use of GOSAT-retrieved X$_{ratio}$ for constraining the surface fluxes of CO$_2$ and CH$_4$. First, we validated the XCH$_4$, XCO$_2$, and X$_{ratio}$ retrievals, as well as the model-derived XCO$_2$ fields used in the proxy methods, using TCCON measurements. This analysis confirmed that biases in non-scattering XCH$_4$ and XCO$_2$ retrievals largely cancel out in X$_{ratio}$. X$_{ratio}$ has a larger mean bias than model-derived XCO$_2$ from CarbonTracker and MACC, suggesting that mostly retrieval biases, rather than CO$_2$ model errors, limit the performance of the proxy method. This is true, especially at a large temporal and spatial scale. To account for biases in GOSAT-retrieved X$_{ratio}$, a TCCON-derived correction was applied as a function of surface albedo, resulting in a mean adjustment of -0.74 %. An additional correction was applied to X$_{ratio}$, XCH$_4^{ct}$, and XCH$_4^{ma}$ to account for a bias between NOAA-optimized CH$_4$ fields in TM5 and TCCON-observed XCH$_4$, amounting to -0.76, -0.80, and 0.59 %, respectively.

We optimized monthly CH$_4$ and CO$_2$ fluxes for the year 2009 and 2010 by assimilating GOSAT-retrieved X$_{ratio}$ data using the TM5–4DVAR inverse modeling system. Additional inversions, assimilating XCH$_4^{proxy}$ and NOAA surface flask measurements, were performed in a similar setup for comparison. The posterior uncertainties of the fluxes are calculated with a Monte Carlo approach.

Overall, the ratio and proxy inversions show similar results for annual CH$_4$ fluxes. Significant seasonal differences in CH$_4$ are found between the two proxy inversions for TransCom regions northern Africa and Australia, which can be traced back to differences in XCO$_2^{model}$. The CO$_2$ models show a systematic difference in the seasonal cycle of CO$_2$, resulting in a seasonally varying mismatch in the northern tropics. The ratio method has the advantage that it allows adjustment of the CO$_2$ fluxes, whereas the proxy inversions can only account for this mismatch by adjusting CH$_4$. For Australia, the proxy inversions predict an anomalous CH$_4$ increase in the second half of 2010. This difference can be explained by errors in XCO$_2^{model}$, which does not account for the anomalous carbon sink reported by Detmers et al. (2015) for lack of surface measurement coverage. The ratio method has the built-in flexibility needed to attribute the anomaly to CO$_2$ instead of CH$_4$, and is therefore is not affected.

Inversions using satellite data show a better agreement among each other compared to the NOAA-only inversions, which use only surface data. This is true in particular for temperate Eurasia, where the NOAA-only inversion reduces the annual CH$_4$ flux by as much as 55 Tg y^{-1}, relative to an a priori flux of 121 Tg y^{-1}. This is traced back to a large overestimation of atmospheric CH$_4$ concentration in the prior model at NOAA sites in the region, especially at Shangdianzi, where the prior model overestimates the data by 179 ppb on average. When satellite measurements are assimilated, the CH$_4$ flux reduction for temperate Eurasia is

limited to $21\,\text{Tg}\,\text{y}^{-1}$, while accounting for the a priori mismatch in Shangdianzi.

We validated the inversion-optimized atmospheric tracer fields, as well as the CarbonTracker and MACC CO_2 fields used in the proxy inversions, against three independent aircraft measurement projects. For CH_4, the ratio and NOAA-only inversions showed a lower mismatch with HIPPO and AMAZONICA measurements than the two proxy inversions. Further analysis shows that this is not due to a better representation of atmospheric CO_2 in the ratio inversion. However, the ratio inversion accounts for inconsistent constraints from X_{ratio} by correcting both CH_4 and CO_2 fluxes, whereas the proxy inversions can only attribute such constraints to CH_4 fluxes. The ratio inversion predicts an enhanced CO_2 natural source in this region during 2010 compared with the NOAA-only and a priori model. This is in accordance with the findings of Gatti et al. (2014) and Van der Laan et al. (2015), and is also supported by the AMAZONICA aircraft measurements. Overall, this study shows that the ratio method is capable of informing us about surface fluxes of CH_4 and CO_2 using satellite measurements, and that it provides a useful alternative for the proxy inversion method.

Data availability

Level 2 XCH_4 and X_{ratio} data from GOSAT/TANSO are calculated using the RemoTeC algorithm. The data are publicly available from the ESA's Climate Change Initiative website (http://www.esa-ghg-cci.org/). NOAA's GGGRN CH_4 measurements are publically available at ftp://aftp.cmdl.noaa.gov/data/trace_gases/ch4/flask/surface/. CarbonTracker CO_2 fluxes are provided by NOAA ESRL, Boulder, Colorado, USA from the website at http://carbontracker.noaa.gov.

Appendix A: Bias correction

We apply a two-step correction to reduce the influence of biases in our inversions.

1. TCCON-based: residual biases in X_{ratio} remain that are not accounted for by calculating the ratio between XCH_4^{ns} and XCO_2^{ns}. The standard bias correction procedure in the RemoTeC XCH_4^{proxy} retrieval assumes a linear dependence on surface albedo (Guerlet et al., 2013). However, this procedure would also correct biases in XCO_2^{model}, which are not expected to vary with surface albedo. Therefore, we apply the albedo-based bias correction only to the GOSAT-measured X_{ratio}. To determine the bias correction, we use GOSAT retrievals that are co-located with TCCON measurements; i.e., they are within $5°$ latitude and longitude and within $2\,h$ of TCCON measurements. The relationship between surface albedo at $1593\,nm$ and the monthly difference between GOSAT and TCCON is shown in Fig. A1. A global bias correction function, obtained by linear regression, results in a mean adjustment of -0.74% of GOSAT X_{ratio}.

2. NOAA-based: a systematic mismatch between the NOAA and GOSAT-optimized TM5 CH_4 fields has been discussed in Monteil et al. (2013). The cause of this problem is still unresolved, but may be explained in part by transport model uncertainties in representing XCH_4 in the stratosphere. Several other studies have reported similar biases and applied NOAA-based bias corrections, in addition to the TCCON-derived retrieval corrections in order to restore consistency between the observational constraints provided by surface and total column measurements (Alexe et al., 2015; Houweling et al., 2014; Basu et al., 2013). We use a similar procedure for X_{ratio} and XCH_4^{proxy} data by comparing the TCCON-corrected GOSAT retrievals to the NOAA-optimized TM5 model. The mean difference is corrected using a linear function of latitude. This results in a mean adjustment of -0.76% in X_{ratio}, -0.59% in XCH_4^{ma}, and -0.80% in XCH_4^{ct} (see Figs. A2 and A3).
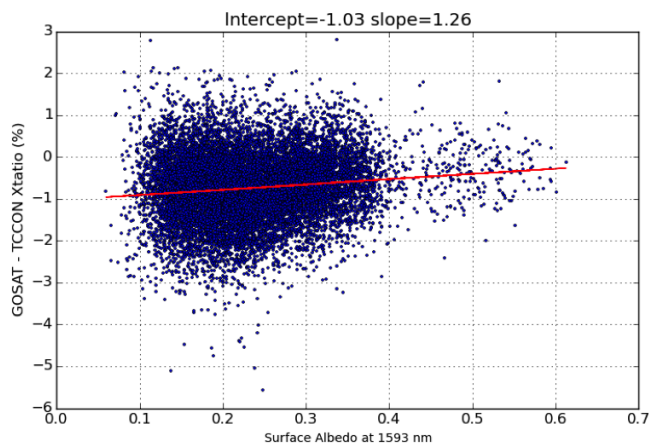

Figure A1. Linear regression analysis between GOSAT–TCCON X_{ratio} and surface albedo at $1593\,nm$.
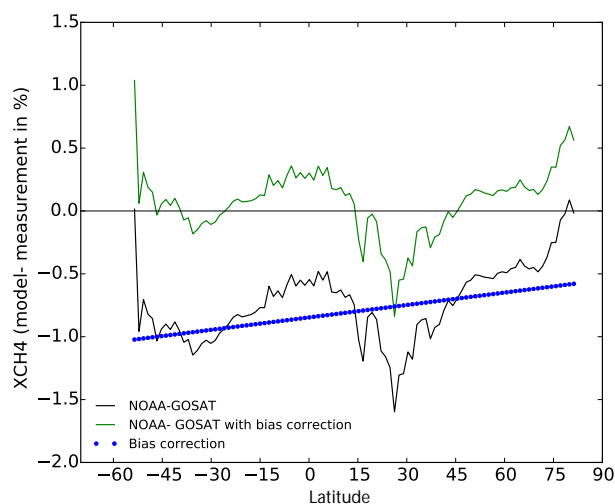

Figure A2. NOAA-based bias correction applied to XCH_4 in the PR-CT inversion.
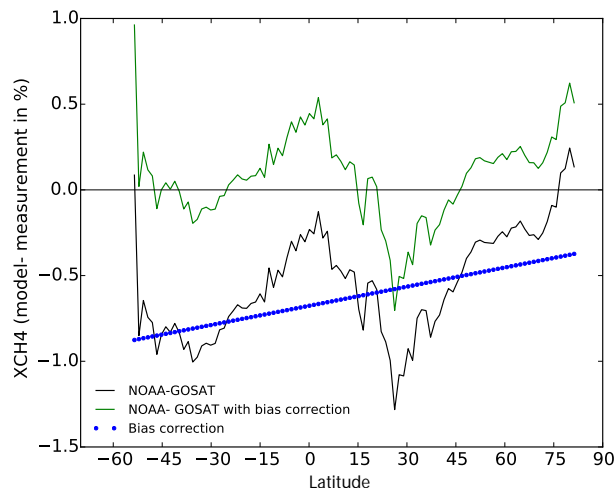

Figure A3. NOAA-based bias correction applied to X_{ratio} in the RATIO inversion.

Appendix B: Posterior uncertainty

As discussed in Pandey et al. (2015), the X$_{ratio}$ inversion problem is weakly nonlinear and is solved using the quasi-Newtonian optimizer M1QN3. The standard implementation of M1QN3 does not provide an estimate of posterior uncertainties. Therefore, we use the Monte Carlo approach as described in Chevallier et al. (2007) to calculate posterior flux uncertainties. For the linear SURF and proxy inversions, we use the conjugate gradient optimization method. The posterior flux uncertainties of these inversions are derived using the same approach to keep the comparison between the uncertainties consistent. A sensitivity test has been performed to determine the size of the ensemble needed to properly capture the 1σ of the prior fluxes. Figure B1 shows the results of this experiment. We choose an ensemble size of 24 for our experiments, which gives a 1σ estimate with 14.4 % uncertainty.
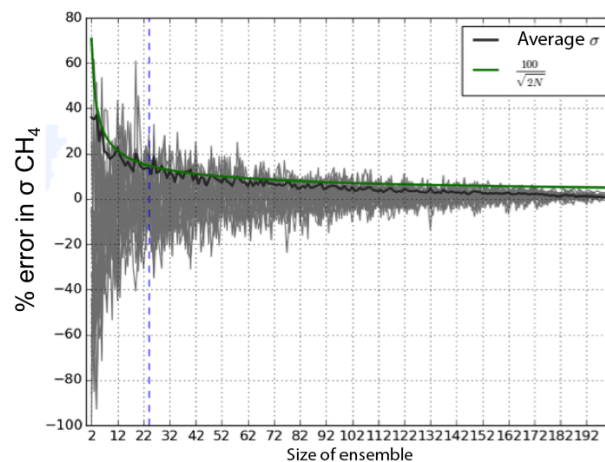

Figure B1. The gray lines represent the percentage error of 1σ of ensemble size n from the σ of ensemble size of 200 of the a priori CH$_4$ flux integrated over TransCom regions. The dark black line represents the average deviation in the gray lines. The green line represents the analytical variation of the error of 1σ (Bousserez et al., 2015). A constant difference of approx. 6 % between the estimates comes from the finite size of the largest sample (200).

The Supplement related to this article is available online at doi:10.5194/acp-16-5043-2016-supplement.

References

Alexe, M., Bergamaschi, P., Segers, A., Detmers, R., Butz, A., Hasekamp, O., Guerlet, S., Parker, R., Boesch, H., Frankenberg, C., Scheepmaker, R. A., Dlugokencky, E., Sweeney, C., Wofsy, S. C., and Kort, E. A.: Inverse modelling of CH_4 emissions for 2010–2011 using different satellite retrieval products from GOSAT and SCIAMACHY, Atmos. Chem. Phys., 15, 113–133, doi:10.5194/acp-15-113-2015, 2015.

Basu, S., Guerlet, S., Butz, A., Houweling, S., Hasekamp, O., Aben, I., Krummel, P., Steele, P., Langenfelds, R., Torn, M., Biraud, S., Stephens, B., Andrews, A., and Worthy, D.: Global CO_2 fluxes estimated from GOSAT retrievals of total column CO_2, Atmos. Chem. Phys., 13, 8695–8717, doi:10.5194/acp-13-8695-2013, 2013.

Basu, S., Krol, M., Butz, A., Clerbaux, C., Sawa, Y., Machida, T., Matsueda, H., Frankenberg, C., Hasekamp, O., and Aben, I.: The seasonal variation of the CO_2 flux over Tropical Asia estimated from GOSAT, CONTRAIL, and IASI, Geophys. Res. Lett., 41, 1809–1815, doi:10.1002/2013GL059105, 2014.

Bergamaschi, P., Frankenberg, C., Meirink, J. F., Krol, M., Dentener, F., Wagner, T., Platt, U., Kaplan, J. O., Körner, S., Heimann, M., Dlugokencky, E. J., and Goede, A.: Satellite chartography of atmospheric methane from SCIAMACHY on board ENVISAT: 2. Evaluation based on inverse model simulations, J. Geophys. Res., 112, D02304, doi:10.1029/2006JD007268, 2007.

Bergamaschi, P., Krol, M., Meirink, J. F., Dentener, F., Segers, A., van Aardenne, J., Monni, S., Vermeulen, A. T., Schmidt, M., Ramonet, M., Yver, C., Meinhardt, F., Nisbet, E. G., Fisher, R. E., O'Doherty, S., and Dlugokencky, E. J.: Inverse modeling of European CH_4 emissions 2001–2006, J. Geophys. Res., 115, D22309, doi:10.1029/2010JD014180, 2010.

Bergamaschi, P., Houweling, S., Segers, A., Krol, M., Frankenberg, C., Scheepmaker, R. A., Dlugokencky, E., Wofsy, S. C., Kort, E. A., Sweeney, C., Schuck, T., Brenninkmeijer, C., Chen, H., Beck, V., and Gerbig, C.: Atmospheric CH_4 in the first decade of the 21st century: Inverse modeling analysis using SCIAMACHY satellite retrievals and NOAA surface measurements, J. Geophys. Res.-Atmos., 118, 7350–7369, doi:10.1002/jgrd.50480, 2013.

Bousquet, P., Ciais, P., Miller, J. B., Dlugokencky, E. J., Hauglustaine, D. A., Prigent, C., Van der Werf, G. R., Peylin, P., Brunke, E.-G., Carouge, C., Langenfelds, R. L., Lathière, J., Papa, F., Ramonet, M., Schmidt, M., Steele, L. P., Tyler, S. C., and White, J.: Contribution of anthropogenic and natural sources to atmospheric methane variability, Nature, 443, 439–43, doi:10.1038/nature05132, 2006.

Bousserez, N., Henze, D. K., Perkins, A., Bowman, K. W., Lee, M., Liu, J., Deng, F., and Jones, D. B. A.: Improved analysis-error covariance matrix for high-dimensional variational inversions: application to source estimation using a 3D atmospheric transport model, Q. J. Roy. Meteor. Soc., 141, 1906–1921, doi:10.1002/qj.2495, 2015.

Bruhwiler, L., Dlugokencky, E., Masarie, K., Ishizawa, M., Andrews, A., Miller, J., Sweeney, C., Tans, P., and Worthy, D.: CarbonTracker-CH_4: an assimilation system for estimating emissions of atmospheric methane, Atmos. Chem. Phys., 14, 8269–8293, doi:10.5194/acp-14-8269-2014, 2014.

Butz, A., Hasekamp, O. P., Frankenberg, C., Vidot, J., and Aben, I.: CH_4 retrievals from space-based solar backscatter measurements: Performance evaluation against simulated aerosol and cirrus loaded scenes, J. Geophys. Res., 115, D24302, doi:10.1029/2010JD014514, 2010.

Butz, A., Guerlet, S., and Hasekamp, O.: Toward accurate CO_2 and CH_4 observations from GOSAT, Geophys. Res. Lett., 38, L14812, doi:10.1029/2011GL047888, 2011.

Chevallier, F.: On the parallelization of atmospheric inversions of CO_2 surface fluxes within a variational framework, Geosci. Model Dev., 6, 783–790, doi:10.5194/gmd-6-783-2013, 2013.

Chevallier, F., Bréon, F.-M., and Rayner, P. J.: Contribution of the Orbiting Carbon Observatory to the estimation of CO_2 sources and sinks: Theoretical study in a variational data assimilation framework, J. Geophys. Res., 112, D09307, doi:10.1029/2006JD007375, 2007.

Chevallier, F., Ciais, P., Conway, T. J., Aalto, T., Anderson, B. E., Bousquet, P., Brunke, E. G., Ciattaglia, L., Esaki, Y., Fröhlich, M., Gomez, A., Gomez-Pelaez, A. J., Haszpra, L., Krummel, P. B., Langenfelds, R. L., Leuenberger, M., Machida, T., Maignan, F., Matsueda, H., Morguí, J. A., Mukai, H., Nakazawa, T., Peylin, P., Ramonet, M., Rivier, L., Sawa, Y., Schmidt, M., Steele, L. P., Vay, S. A., Vermeulen, A. T., Wofsy, S., and Worthy, D.: CO_2 surface fluxes at grid point scale estimated from a global 21 year reanalysis of atmospheric measurements, J. Geophys. Res., 115, D21307, doi:10.1029/2010JD013887, 2010.

Chevallier, F., Palmer, P., Feng, L., Boesch, H., O'Dell, C., and Bousquet, P.: Toward robust and consistent regional CO_2 flux estimates from in situ and spaceborne measurements of atmospheric CO_2, Geophys. Res. Lett., 41, 1065–1070, doi:10.1002/2013GL058772, 2014.

Dee, D. P., Uppala, S. M., Simmons, A. J., Berrisford, P., Poli, P., Kobayashi, S., Andrae, U., Balmaseda, M. A., Balsamo, G., Bauer, P., Bechtold, P., Beljaars, A. C. M., van de Berg, L., Bidlot, J., Bormann, N., Delsol, C., Dragani, R., Fuentes, M., Geer, A. J., Haimberger, L., Healy, S. B., Hersbach, H., Hólm, E. V., Isaksen, L., Kållberg, P., Köhler, M., Matricardi, M., McNally, A. P., Monge-Sanz, B. M., Morcrette, J.-J., Park, B.-K., Peubey, C., de Rosnay, P., Tavolato, C., Thépaut, J.-N., and Vitart, F.: The ERA-Interim reanalysis: configuration and performance of the

data assimilation system, Q. J. Roy. Meteor. Soc., 137, 553–597, doi:10.1002/qj.828, 2011.

Deng, F., Jones, D. B. A., Henze, D. K., Bousserez, N., Bowman, K. W., Fisher, J. B., Nassar, R., O'Dell, C., Wunch, D., Wennberg, P. O., Kort, E. A., Wofsy, S. C., Blumenstock, T., Deutscher, N. M., Griffith, D. W. T., Hase, F., Heikkinen, P., Sherlock, V., Strong, K., Sussmann, R., and Warneke, T.: Inferring regional sources and sinks of atmospheric CO_2 from GOSAT XCO_2 data, Atmos. Chem. Phys., 14, 3703–3727, doi:10.5194/acp-14-3703-2014, 2014.

Detmers, R. and Hasekamp, O.: RemoTeC XCH4 PROXY GOSAT Data Products, SRON-Netherlands Institute for Space Research, available at: www.esa-ghg-cci.org/?q=webfm_send/180, last access: 20 October 2014.

Detmers, R. G., Hasekamp, O., Aben, I., Houweling, S., Leeuwen, T. T. V., and Butz, A.: Anomalous carbon uptake in Australia as seen by GOSAT, Geophys. Res. Lett., 42, 8177–8184, doi:10.1002/2015GL065161, 2015.

Deutscher, N., Notholt, J., Messerschmidt, J., Weinzierl, C., Warneke, T., Petri, C., Grupe, P., and Katrynski, K.: TCCON Data Archive, hosted by the Carbon Dioxide Information Analysis Center, Oak Ridge National Laboratory, Oak Ridge, Tennessee, USA, doi:10.14291/tccon.ggg2014.bialystok01.R0/1149277, 2014a.

Deutscher, N., Notholt, J., Messerschmidt, J., Weinzierl, C., Warneke, T., Petri, C., Grupe, P., and Katrynski, K.: TCCON data from Bialystok, Poland, Release GGG2014R0. TCCON data archive, hosted by the Carbon Dioxide Information Analysis Center, Oak Ridge National Laboratory, Oak Ridge, Tennessee, USA, doi:10.14291/tccon.ggg2014.bremen01.R0/1149275, 2014b.

Dlugokencky, E. J., Lang, P. M., Crotwell, A. M., Masarie, K. A., and Crotwell, M. J.: Atmospheric Methane Dry Air Mole Fractions from the NOAA ESRL Carbon Cycle Cooperative Global Air Sampling Network, 1983–2014, Version: 2015-08-03, available at: ftp://aftp.cmdl.noaa.gov/data/trace_gases/ch4/flask/surface/ (last access: 20 October 2014), 2015.

Frankenberg, C., Meirink, J. F., van Weele, M., Platt, U., and Wagner, T.: Assessing methane emissions from global space-borne observations, Science, 308, 1010–1014, doi:10.1126/science.1106644, 2005.

Frankenberg, C., Meirink, J. F., Bergamaschi, P., Goede, A. P. H., Heimann, M., Körner, S., Platt, U., van Weele, M., and Wagner, T.: Satellite chartography of atmospheric methane from SCIAMACHY on board ENVISAT: Analysis of the years 2003 and 2004, J. Geophys. Res.-Atmos., 111, D07303, doi:10.1029/2005JD006235, 2006.

Fraser, A., Palmer, P. I., Feng, L., Boesch, H., Cogan, A., Parker, R., Dlugokencky, E. J., Fraser, P. J., Krummel, P. B., Langenfelds, R. L., O'Doherty, S., Prinn, R. G., Steele, L. P., van der Schoot, M., and Weiss, R. F.: Estimating regional methane surface fluxes: the relative importance of surface and GOSAT mole fraction measurements, Atmos. Chem. Phys., 13, 5697–5713, doi:10.5194/acp-13-5697-2013, 2013.

Fraser, A., Palmer, P. I., Feng, L., Bösch, H., Parker, R., Dlugokencky, E. J., Krummel, P. B., and Langenfelds, R. L.: Estimating regional fluxes of CO_2 and CH_4 using space-borne observations of $XCH_4 : XCO_2$, Atmos. Chem. Phys., 14, 12883–12895, doi:10.5194/acp-14-12883-2014, 2014.

Gatti, L. V., Gloor, M., Miller, J. B., Doughty, C. E., Malhi, Y., Domingues, L. G., Basso, L. S., Martinewski, A., Correia, C. S. C., Borges, V. F., Freitas, S., Braz, R., Anderson, L. O., Rocha, H., Grace, J., Phillips, O. L., and Lloyd, J.: Drought sensitivity of Amazonian carbon balance revealed by atmospheric measurements., Nature, 506, 76–80, doi:10.1038/nature12957, 2014.

Griffith, D. W. T., Deutscher, N., Velazco, V. A., Wennberg, P. O., Yavin, Y., Aleks, G. K., Washenfelder, R., Toon, G. C., Blavier, J.-F., Murphy, C., Jones, N., Kettlewell, G., Connor, B., Macatangay, R., Roehl, C., Ryczek, M., Glowacki, J., Culgan, T., and Bryant, G.: TCCON Data from Darwin, Australia, Release GGG2014R0. TCCON Data Archive, hosted by the Carbon Dioxide Information Analysis Center, Oak Ridge National Laboratory, Oak Ridge, Tennessee, USA, doi:10.14291/tccon.ggg2014.darwin01.R0/1149290, 2014a.

Griffith, D. W. T., Velazco, V. A., Deutscher, N., Murphy, C., Jones, N., Wilson, S., Macatangay, R., Kettlewell, G., Buchholz, R. R., and Riggenbach, M.: TCCON Data from Wollongong, Australia, Release GGG2014R0. TCCON Data Archive, hosted by the Carbon Dioxide Information Analysis Center, Oak Ridge National Laboratory, Oak Ridge, Tennessee, USA, doi:10.14291/tccon.ggg2014.wollongong01.R0/1149291, 2014b.

Guerlet, S., Butz, A., Schepers, D., Basu, S., Hasekamp, O. P., Kuze, A., Yokota, T., Blavier, J. F., Deutscher, N. M., Griffith, D. W. T., Hase, F., Kyro, E., Morino, I., Sherlock, V., Sussmann, R., Galli, A., and Aben, I.: Impact of aerosol and thin cirrus on retrieving and validating XCO_2 from GOSAT shortwave infrared measurements, J. Geophys. Res.-Atmos., 118, 4887–4905, doi:10.1002/jgrd.50332, 2013.

Gurney, K. R., Baker, D., Rayner, P., and Denning, S.: Interannual variations in continental-scale net carbon exchange and sensitivity to observing networks estimated from atmospheric CO_2 inversions for the period 1980 to 2005, Global Biogeochem. Cy., 22, GB3025, doi:10.1029/2007GB003082, 2008.

Hase, F., Blumenstock, T., Dohe, S., Groß, J., and Kiel, M.: TCCON Data from Karlsruhe, Germany, Release GGG2014R0, TCCON Data Archive, hosted by the Carbon Dioxide Information Analysis Center, Oak Ridge National Laboratory, Oak Ridge, Tennessee, USA, doi:10.14291/tccon.ggg2014.karlsruhe01.R0/1149270, 2014.

Hein, R., Crutzen, P. J., and Heimann, M.: An inverse modeling approach to investigate the global atmospheric methane cycle, Global Biogeochem. Cy., 11, 43–76, doi:10.1029/96GB03043, 1997.

Houweling, S., Kaminski, T., Dentener, F., Lelieveld, J., and Heimann, M.: Inverse modeling of methane sources and sinks using the adjoint of a global transport model, J. Geophys. Res., 104, 26137–26160, 1999.

Houweling, S., Breon, F.-M., Aben, I., Rödenbeck, C., Gloor, M., Heimann, M., and Ciais, P.: Inverse modeling of CO_2 sources and sinks using satellite data: a synthetic inter-comparison of measurement techniques and their performance as a function of space and time, Atmos. Chem. Phys., 4, 523–538, doi:10.5194/acp-4-523-2004, 2004.

Houweling, S., Krol, M., Bergamaschi, P., Frankenberg, C., Dlugokencky, E. J., Morino, I., Notholt, J., Sherlock, V., Wunch, D., Beck, V., Gerbig, C., Chen, H., Kort, E. A., Röckmann, T., and Aben, I.: A multi-year methane inversion using SCIAMACHY,

accounting for systematic errors using TCCON measurements, Atmos. Chem. Phys., 14, 3991–4012, doi:10.5194/acp-14-3991-2014, 2014.

Houweling, S., Baker, D., Basu, S., Boesch, H., Butz, A., Chevallier, F., Deng, F., Dlugokencky, E. J., Feng, L., Ganshin, A., Hasekamp, O., Jones, D., Maksyutov, S., Marshall, J., Oda, T., Dell, C. W. O., Oshchepkov, S., Palmer, P. I., Peylin, P., Poussi, Z., Reum, F., Takagi, H., Yoshida, Y., and Zhuravlev, R.: An intercomparison of inverse models for estimating sources and sinks of CO$_2$ using GOSAT measurements, J. Geophys. Res., 120, 5253–5266, doi:10.1002/2014JD022962, 2015.

Jacobson, A. R., Mikaloff Fletcher, S. E., Gruber, N., Sarmiento, J. L., and Gloor, M.: A joint atmosphere-ocean inversion for surface fluxes of carbon dioxide: 1. Methods and global-scale fluxes, Global Biogeochem. Cy., 21, GB1019, doi:10.1029/2005GB002556, 2007.

Kivi, R., Heikkinen, P., and Kyro, E.: TCCON Data from Sodankyla, Finland, Release GGG2014R0. TCCON Data Archive, hosted by the Carbon Dioxide Information Analysis Center, Oak Ridge National Laboratory, Oak Ridge, Tennessee, USA, doi:10.14291/tccon.ggg2014.sodankyla01.R0/1149280, 2014.

Krol, M., Houweling, S., Bregman, B., van den Broek, M., Segers, A., van Velthoven, P., Peters, W., Dentener, F., and Bergamaschi, P.: The two-way nested global chemistry-transport zoom model TM5: algorithm and applications, Atmos. Chem. Phys., 5, 417–432, doi:10.5194/acp-5-417-2005, 2005.

Kuze, A., Suto, H., Nakajima, M., and Hamazaki, T.: Thermal and near infrared sensor for carbon observation Fourier-transform spectrometer on the Greenhouse Gases Observing Satellite for greenhouse gases monitoring, Appl. Optics, 48, 6716–6733, doi:10.1364/AO.48.006716, 2009.

Machida, T., Matsueda, H., Sawa, Y., Nakagawa, Y., Hirotani, K., Kondo, N., Goto, K., Nakazawa, T., Ishikawa, K., and Ogawa, T.: Worldwide Measurements of Atmospheric CO$_2$ and Other Trace Gas Species Using Commercial Airlines, J. Atmos. Ocean. Tech., 25, 1744–1754, doi:10.1175/2008JTECHA1082.1, 2008.

Maksyutov, S., Takagi, H., Belikov, D. A., Saeki, T., Zhuravlev, R., Ganshin, A., Lukyanov, A., Yoshida, Y., Oshchepkov, S., Bril, A., Saito, M., Oda, T., Valsala, V. K., Saito, R., Andres, R. J., Conway, T., Tans, P., and Yokota, T.: Estimation of regional surface CO$_2$ fluxes with GOSAT observations using two inverse modeling approaches, Proc. SPIE 8529, Remote Sensing and Modeling of the Atmosphere, Oceans, and Interactions IV, 85290G, doi:10.1117/12.979664, 2012.

Meirink, J. F., Bergamaschi, P., and Krol, M. C.: Four-dimensional variational data assimilation for inverse modelling of atmospheric methane emissions: method and comparison with synthesis inversion, Atmos. Chem. Phys., 8, 6341–6353, doi:10.5194/acp-8-6341-2008, 2008.

Monteil, G., Houweling, S., Butz, A., Guerlet, S., Schepers, D., Hasekamp, O., Frankenberg, C., Scheepmaker, R., Aben, I., and Röckmann, T.: Comparison of CH$_4$ inversions based on 15 months of GOSAT and SCIAMACHY observations, J. Geophys. Res.-Atmos., 118, 11807–11823, doi:10.1002/2013JD019760, 2013.

Morino, I., Matsuzaki, T., Ikegami, H., and Shishime, A.: TCCON data from Tsukuba, Ibaraki, Japan, 120HR, Release GGG2014R0. TCCON data archive, hosted by the Carbon Dioxide Information Analysis Center, Oak Ridge National Laboratory, Oak Ridge, Tennessee, USA, doi:10.14291/tccon.ggg2014.tsukuba01.R0/1149281, 2014.

Palmer, P. I., Suntharalingam, P., Jones, D. B. A., Jacob, D. J., Streets, D. G., Fu, Q., Vay, S. A., and Sachse, G. W.: Using CO$_2$: CO correlations to improve inverse analyses of carbon fluxes, J. Geophys. Res., 111, D12318, doi:10.1029/2005JD006697, 2006.

Pandey, S., Houweling, S., Krol, M., Aben, I., and Röckmann, T.: On the use of satellite-derived CH$_4$: CO$_2$ columns in a joint inversion of CH$_4$ and CO$_2$ fluxes, Atmos. Chem. Phys., 15, 8615–8629, doi:10.5194/acp-15-8615-2015, 2015.

Parker, R. J., Boesch, H., Byckling, K., Webb, A. J., Palmer, P. I., Feng, L., Bergamaschi, P., Chevallier, F., Notholt, J., Deutscher, N., Warneke, T., Hase, F., Sussmann, R., Kawakami, S., Kivi, R., Griffith, D. W. T., and Velazco, V.: Assessing 5 years of GOSAT Proxy XCH$_4$ data and associated uncertainties, Atmos. Meas. Tech., 8, 4785–4801, doi:10.5194/amt-8-4785-2015, 2015.

Peters, W., Jacobson, A. R., Sweeney, C., Andrews, A. E., Conway, T. J., Masarie, K., Miller, J. B., Bruhwiler, L. M. P., Pétron, G., Hirsch, A. I., Worthy, D. E. J., van der Werf, G. R., Randerson, J. T., Wennberg, P. O., Krol, M. C., and Tans, P. P.: An atmospheric perspective on North American carbon dioxide exchange: CarbonTracker, P. Natl. Acad. Sci. USA, 104, 18925–18930, doi:10.1073/pnas.0708986104, 2007.

Reuter, M., Buchwitz, M., Hilker, M., Heymann, J., Schneising, O., Pillai, D., Bovensmann, H., Burrows, J. P., Bösch, H., Parker, R., Butz, A., Hasekamp, O., O'Dell, C. W., Yoshida, Y., Gerbig, C., Nehrkorn, T., Deutscher, N. M., Warneke, T., Notholt, J., Hase, F., Kivi, R., Sussmann, R., Machida, T., Matsueda, H., and Sawa, Y.: Satellite-inferred European carbon sink larger than expected, Atmos. Chem. Phys., 14, 13739–13753, doi:10.5194/acp-14-13739-2014, 2014.

Schepers, D., Guerlet, S., Butz, A., Landgraf, J., Frankenberg, C., Hasekamp, O., Blavier, J.-F., Deutscher, N. M., Griffith, D. W. T., Hase, F., Kyro, E., Morino, I., Sherlock, V., Sussmann, R., and Aben, I.: Methane retrievals from Greenhouse Gases Observing Satellite (GOSAT) shortwave infrared measurements: Performance comparison of proxy and physics retrieval algorithms, J. Geophys. Res., 117, D10307, doi:10.1029/2012JD017549, 2012.

Sherlock, V., Connor, B., Robinson, J., Shiona, H., Smale, D., and Pollard, D.: TCCON Data from Lauder, New Zealand, 120HR, Release GGG2014R0. TCCON Data Archive, hosted by the Carbon Dioxide Information Analysis Center, Oak Ridge National Laboratory, Oak Ridge, Tennessee, USA, doi:10.14291/tccon.ggg2014.lauder01.R0/1149293, 2014.

Spahni, R., Wania, R., Neef, L., van Weele, M., Pison, I., Bousquet, P., Frankenberg, C., Foster, P. N., Joos, F., Prentice, I. C., and van Velthoven, P.: Constraining global methane emissions and uptake by ecosystems, Biogeosciences, 8, 1643–1665, doi:10.5194/bg-8-1643-2011, 2011.

Sussmann, R. and Rettinger, M.: TCCON Data from Garmisch, Germany, Release GGG2014R0. TCCON Data Archive, hosted by the Carbon Dioxide Information Analysis Center, Oak Ridge National Laboratory, Oak Ridge, Tennessee, USA, doi:10.14291/tccon.ggg2014.garmisch01.R0/1149299, 2014.

Tans, P., Jacobson, A., Schuldt, K., Mund, J., Trudeau, M., Peters, W., Andrews, A., Sweeney, C., Miller, J. B., Oda, T., Bruhwiler, L., and Pétron, G.: CarbonTracker CO$_2$ fluxes, NOAA ESRL,

Boulder, Colorado, USA, available at: http://carbontracker.noaa.gov, last access: 15 June 2014.

Thompson, R. L., Stohl, A., Zhou, L. X., Dlugokencky, E., Fukuyama, Y., Tohjima, Y., Kim, S., Lee, H., Nisbet, E. G., Fisher, R. E., Lowry, D., Weiss, R. F., Prinn, R. G., Doherty, S. O., Young, D., and White, J. W. C.: Methane emissions in East Asia for 2000–2011 estimated using an atmospheric Bayesian inversion, J. Geophys. Res., 120, 4352–4369, doi:10.1002/2014JD022394, 2015.

Turner, A. J., Jacob, D. J., Wecht, K. J., Maasakkers, J. D., Lundgren, E., Andrews, A. E., Biraud, S. C., Boesch, H., Bowman, K. W., Deutscher, N. M., Dubey, M. K., Griffith, D. W. T., Hase, F., Kuze, A., Notholt, J., Ohyama, H., Parker, R., Payne, V. H., Sussmann, R., Sweeney, C., Velazco, V. A., Warneke, T., Wennberg, P. O., and Wunch, D.: Estimating global and North American methane emissions with high spatial resolution using GOSAT satellite data, Atmos. Chem. Phys., 15, 7049–7069, doi:10.5194/acp-15-7049-2015, 2015.

Van der Laan-Luijkx, I. T., Van der Velde, I. R., Krol, M. C., Gatti, L. V., Domingues, L. G., Correia, C. S. C., Miller, J. B., Gloor, M., Leeuwen, T. T., Kaiser, J. W., Wiedinmyer, C., Basu, S., Clerbaux, C., and Peters, W.: Response of the Amazon carbon balance to the 2010 drought derived with CarbonTracker South America, Global Biogeochem. Cy., 29, 1–17, doi:10.1002/2014GB005082, 2015.

Warneke, T., Messerschmidt, J., Notholt, J., Weinzierl, C., Deutscher, N., Petri, C., Grupe, P., Vuillemin, C., Truong, F., Schmidt, M., Ramonet, M., and Parmentier, E.: TCCON Data from Orleans, France, Release GGG2014R0. TCCON Data Archive, hosted by the Carbon Dioxide Information Analysis Center, Oak Ridge National Laboratory, Oak Ridge, Tennessee, USA, doi:10.14291/tccon.ggg2014.orleans01.R0/1149276, 2014.

Wennberg, P. O., Roehl, C., Wunch, D., Toon, G. C., Blavier, J.-F., Washenfelder, R., Keppel-Aleks, G., Allen, N., and Ayers, J.: TCCON data from Park Falls, Wisconsin, USA, Release GGG2014R0. TCCON data archive, hosted by the Carbon Dioxide Information Analysis Center, Oak Ridge National Laboratory, Oak Ridge, Tennessee, USA, doi:10.14291/tccon.ggg2014.parkfalls01.R0/1149161, 2014a.

Wennberg, P. O., Wunch, D., Roehl, C., Blavier, J.-F., Toon, G. C., Allen, N., Dowell, P., Teske, K., Martin, C., and Martin, J.: TCCON Data from Lamont, Oklahoma, USA, Release GGG2014R0. TCCON Data Archive, hosted by the Carbon Dioxide Information Analysis Center, Oak Ridge National Laboratory, Oak Ridge, Tennessee, USA, doi:10.14291/tccon.ggg2014.lamont01.R0/1149159, 2014b.

Wofsy, S. C., Daube, B. C., Jimenez, R., Kort, E., Pittman, J. V., Park, S., Commane, R., Xiang, B., Santoni, G., Jacob, D., Fisher, J., Pickett-Heaps, C., Wang, H., Wecht, K., Wang, Q.-Q., Stephens, B. B., Shertz, S., Watt, A., Romashkin, P., Campos, T., Haggerty, J., Cooper, W. A., Rogers, D., Beaton, S., Hendershot, R., Elkins, J. W., Fahey, D. W., Gao, R. S., Moore, F., Montzka, S. A., Schwarz, J. P., Perring, A. E., Hurst, D., Miller, B. R., Sweeney, C., Oltmans, S., Nance, D., Hintsa, E., Dutton, G., Watts, L. A., Spackman, J. R., Rosenlof, K. H., Ray, E. A., Hall, B., Zondlo, M. A., Diao, M., Keeling, R., Bent, J., Atlas, E. L., Lueb, R., and Mahoney, M. J.: HIPPO Merged 10-second Meteorology, Atmospheric Chemistry, Aerosol Data (R_20121129). Carbon Dioxide Information Analysis Center, Oak Ridge National Laboratory, Oak Ridge, Tennessee, USA, doi:10.3334/CDIAC/hippo_010, 2012a.

Wofsy, S. C., Daube, B. C., Jimenez, R., Kort, E., Pittman, J. V., Park, S., Commane, R., Xiang, B., Santoni, G., Jacob, D., Fisher, J., Pickett-Heaps, C., Wang, H., Wecht, K., Wang, Q.-Q., Stephens, B. B., Shertz, S., Watt, A., Romashkin, P., Campos, T., Haggerty, J., Cooper, W. A., Rogers, D., Beaton, S., Hendershot, R., Elkins, J. W., Fahey, D. W., Gao, R. S., Moore, F., Montzka, S. A., Schwarz, J. P., Perring, A. E., Hurst, D., Miller, B. R., Sweeney, C., Oltmans, S., Nance, D., Hintsa, E., Dutton, G., Watts, L. A., Spackman, J. R., Rosenlof, K. H., Ray, E. A., Hall, B., Zondlo, M. A., Diao, M., Keeling, R., Bent, J., Atlas, E. L., Lueb, R., and Mahoney, M. J.: HIPPO NOAA Flask Sample GHG, Halocarbon, and Hydrocarbon Data (R_20121129). Carbon Dioxide Information Analysis Center, Oak Ridge National Laboratory, Oak Ridge, Tennessee, USA, doi:10.3334/CDIAC/hippo_013, 2012b.

Wunch, D., Toon, G. C., Blavier, J.-F. L., Washenfelder, R. A., Notholt, J., Connor, B. J., Griffith, D. W. T., Sherlock, V., and Wennberg, P. O.: The total carbon column observing network, Philos. T. R. Soc. A, 369, 2087–112, doi:10.1098/rsta.2010.0240, 2011.

Yokota, T., Yoshida, Y., Eguchi, N., Ota, Y., Tanaka, T., Watanabe, H., and Maksyutov, S.: Global Concentrations of CO$_2$ and CH$_4$ Retrieved from GOSAT: First Preliminary Results, SOLA, 5, 160–163, doi:10.2151/sola.2009-041, 2009.

Yoshida, Y., Ota, Y., Eguchi, N., Kikuchi, N., Nobuta, K., Tran, H., Morino, I., and Yokota, T.: Retrieval algorithm for CO$_2$ and CH$_4$ column abundances from short-wavelength infrared spectral observations by the Greenhouse gases observing satellite, Atmos. Meas. Tech., 4, 717–734, doi:10.5194/amt-4-717-2011, 2011.